Spin-polaron band structure and hole pockets in underdoped cuprates

P. Wróbel,[1] W. Suleja,[1] and R. Eder[2]
[1]*Institute for Low Temperature and Structure Research, P.O. Box 1410, 50-950 Wrocław 2, Poland*
[2]*Forschungszentrum Karlsruhe, Institut für Festkörperphysik, P.O. Box 3640, D-76021 Karlsruhe, Germany*
(Received 21 November 2007; revised manuscript received 26 May 2008; published 1 August 2008)

We present a variational approach based on the string picture to analyze the internal structure and dispersion of spin polarons with different symmetries in an antiferromagnet. We then use this to discuss the properties of underdoped cuprate superconductor within the "doped insulator" picture. The theory explains the remnant Fermi surface for the undoped compounds, as well as hole pockets, Fermi arcs, high-energy pseudogap, and the midinfrared band in doped materials. Destructive interference between the phases of a photohole near Γ and the internal phases of the Zhang-Rice singlet combined with our theory moreover explains the "waterfall" phenomenon.

DOI: 10.1103/PhysRevB.78.064501 PACS number(s): 74.72.−h, 75.50.Ee, 71.27.+a, 71.10.Fd

I. INTRODUCTION

Since the discovery of high-temperature superconductivity (HTSC) in doped antiferromagnetic (AF) insulators, the research on that phenomenon concentrates to a great extent on the properties of single-particle-like excitations in such systems. It is also obvious that the microscopic mechanism of HTSC should hinge on the interaction between quasiparticles. At half-filling the Hubbard model, which is a generic model used to describe strongly correlated systems, is an insulator for large enough U/t (Ref. 1) whereas for low electron density the model is expected to be a Fermi liquid with a Fermi-surface volume in accordance with the Luttinger theorem for any U/t.[2] With increasing doping one might therefore expect a phase transition from a "correlation dominated" phase near half-filling to a Fermi-liquid phase for low density. The key property of the correlation dominated phase thereby is the splitting of the physical electron into the two Hubbard bands which correspond to fermionic holes and double occupancies moving in a "background" of singly occupied sites, whereby the electrons forming the background retain only their spin degrees of freedom. This—and not a half-filled Fermi surface—is the picture underlying all successful theories for the angle-resolved photoemission spectroscopy (ARPES) data[3] obtained in insulating compounds.[4–12] The question then is to what extent these Hubbard bands can be doped before the two-band structure collapses, the spin background "melts" into a Fermi sea, and the Luttinger Fermi surface is regained. The key property of this "doped insulator" phase should be a Fermi surface with a volume proportional to the number of doped holes because these are the only mobile fermions.

ARPES on cuprate superconductors has produced a wealth of information[13] although it has proven difficult to extract a consistent picture. From spectra taken near optimal doping it was concluded that ARPES shows evidence for a "large" Fermi surface consistent with the Luttinger theorem and band calculations[13] which would imply that the doped Hubbard bands never exist. Surprisingly enough, however, insulating compounds such as $Sr_2CuO_2Cl_2$ seemed to show a very similar Fermi surface as well—which has been termed the "remnant Fermi surface."[14] ARPES spectra from insulators show a band which disperses toward lower binding energy and then rapidly looses weight just as if it would cross a Fermi level. The only possible explanation for this phenomenon is a strong and systematic variation of the spectral weight of the conduction band which drops to near zero abruptly at a line in **k** space which roughly coincides with the noninteracting Fermi surface. One can give simple arguments why such a behavior is to be expected.[15] Since there is no reason why such a strong variation of spectral weight and bands with almost no spectral weight should occur only in insulators, one should be cautioned that Fermi-surface maps for doped compounds may not show the full picture either.

In the underdoped compounds the upper Hubbard band, while rapidly loosing spectral weight, still can be clearly resolved.[16] ARPES shows rather structureless spectra which are usually interpreted in terms of a "high-energy feature" and a "leading-edge shift" or, alternatively, high energy and low-energy pseudogaps.[13] In any case there is definitely no large Fermi surface, instead Fermi-surface maps show "Fermi arcs." Bearing in mind the remnant Fermi surface in the insulators suggests to interpret these arcs as being the inner part of a hole pocket centered on $(\frac{\pi}{2},\frac{\pi}{2})$ with the part of the pocket facing (π,π) having too small spectral weight to be seen in ARPES. Assuming that the electronic structure in the underdoped compound can be described in simplest approximation as holes doped into the quasiparticle band of the insulator moreover would give an explanation for the high-energy pseudogap—the dispersion of the high-energy feature—in that it simply reflects the hole dispersion in the insulator.[13] Such a "strict" rigid-band picture would not explain the low-energy pseudogap or the temperature and doping dependence of either high- or low-energy pseudogap. On the other hand the closing of the pseudogap with increasing doping can be seen already in cluster simulations[17] and it has been pointed out there that the mechanism may be an effective downward renormalization of the t' and t'' terms due to decrease in the spin-correlation length. Moreover, the low-energy pseudogap by its definition in terms of the leading-edge shift has no immediate connection with a dispersion and may be determined, e.g., by T-dependent linewidths as discussed by Storey *et al.*[18]

The compound $Ca_{2-x}Na_xCuO_2Cl_2$ shows rather clear evidence for the doped insulator picture[19] in that the dispersion

in the doped case is virtually identical to that in the undoped compound and even the part of the quasiparticle band facing (π,π) may have been observed. Very recently ARPES experiments seem to have provided direct evidence for hole pockets in $La_{1.48}Nd_{0.4}Sr_{0.12}CuO_4$,[20] with the part of the pockets facing (π,π) indeed having small spectral weight—as one would have expected on the basis of the remnant Fermi surface.

It had been noted early on[21] that hole pockets with a volume proportional to the hole concentration would explain the scaling of the low-temperature Hall constant with hole concentration in the underdoped materials[22,23] and that the apparent discrepancy between the "small Fermi surface" suggested by transport measurements and the "large Fermi surface" seen in ARPES may be due to a systematic variation of the quasiparticle weight along the hole pocket.[24] While the recent discovery[25–27] of Shubnikov–de Haas oscillations in some underdoped compounds initially seemed to provide strong evidence for hole pockets, the finding that the oscillations are likely caused by electronlike rather than holelike pockets[28] has complicated matters again.

Lastly, exact diagonalization studies of the t-J model provide clear evidence that the Fermi surface for hole dopings around 10% takes the form of hole pockets.[29,30] Careful analysis of exact diagonalization results shows that in the single particle the spectral function for the doped t-J model is quite consistent with rigid-band filling of the quasiparticle band seen at half-filling, provided one takes into account the formation of hole pairs.[24] By calculating the spectral function for dressed hole operators[31] rather than the bare electron operators can moreover be shown that the quasiparticles in the doped system have very nearly the same internal structure as in the undoped one.[32]

Here we take the point of view that the underdoped regime in high-temperature superconductors precisely corresponds to the doped insulator phase. We show that many properties of the underdoped phase—the remnant Fermi surface, the Fermi arcs, the high-energy feature seen in ARPES, and the midinfrared band seen in the optical conductivity—find a simple and natural explanation in the dispersion and internal structure of the quasiparticles which correspond to holes heavily dressed by spin excitations. Since there are indications that the heavily overdoped phase is essentially a Fermi liquid this would imply that the phase transition from the correlation dominated phase to the Fermi-liquid phase occurs at optimal doping. This would then be a quantum phase transition where none of the two phases has any kind of order—rather they differ in the topology and volume of their Fermi surfaces. An indication of this transition can in fact be seen in the dynamical spin and density correlation function obtained by exact diagonalization of small clusters. In the underdoped regime spin and density correlation functions are very different and the density correlation function takes the form of extended incoherent continua.[33] This form of the density correlation function can be explained quantitatively within the string picture for a single hole.[34] For doping levels higher than optimal, spin and density correlation functions become similar and can be explained well as particle-hole transitions across an essentially free-electronlike Fermi surface.[35]

While a theory for such a transition would be highly desirable but very challenging the present paper has a more modest goal: we want to show that many features of undoped and underdoped cuprates can be explained by a very simple theory which assumes continuity with the insulator. The calculation will be performed in the framework of the t-J model[36,37] extended by terms enabling hopping to second and third nearest neighbors (NNs) with hopping integrals t' and t'', respectively.[38,39] We use standard values $t=0.35$ eV, $t'=-0.12$ eV, $t''=0.08$ eV, and $J=0.14$ eV chosen so as to reproduce the measured Fermi surface of hole doped cuprates for high doping levels.

II. CONSTRUCTION OF LOCALIZED BASIS STATES

Since we want to study the doped insulator we consider the motion of a single hole in an antiferromagnetically ordered "spin background." All processes analyzed in the following actually require only short-range antiferromagnetic correlations—one may therefore expect that hole motion in a state with short-range antiferromagnetic order but no long-range order will involve very similar processes so that, e.g., the internal structure of the quasiparticles and the dispersion relation of a hole should not change drastically. The construction of spin-polaron (SP) states including the excited states was performed in several earlier publications.[40–44] In order to make this paper self-contained we will now briefly repeat that construction. For definiteness we will assume that a $\downarrow$ spin has been removed from the system and study the motion of the resulting hole. We denote the $\downarrow$ sublattice by A.

To begin with we define $H_0=H_t+H_{\mathrm{Ising}}$ to be the sum of the nearest-neighbor hopping $\propto t$ and the longitudinal part of the Heisenberg exchange,

$$H_t=-t\sum_{\langle i,j\rangle,\sigma}(\hat{c}^{\dagger}_{i\sigma}\hat{c}_{j\sigma}+\mathrm{H.c.}),$$

$$H_{\mathrm{Ising}}=J\sum_{\langle i,j\rangle}\left(S^z_iS^z_j-\frac{n_in_j}{4}\right).$$

H_0 is frequently referred to as the t-J_z model. In a first step, we seek approximate eigenstates of H_0 which are localized due to the string effect.

The mechanism of the string effect is shown in Fig. 1. By creating a hole in the Néel state—i.e., the ground state of H_{Ising}—at site i and acting repeatedly with the hopping term we generate a basis of string states $|\mathcal{P}_i\rangle$, where $\mathcal{P}_i=(i,j,\ \ldots,n)$ is shorthand for the sites $i,j,\ \ldots,n$ visited by the hole. All spins on these sites have been displaced by one lattice spacing and thus are inverted relative to the Néel order.

All $|\mathcal{P}_i\rangle$ are eigenstates of H_{Ising}. Taking the energy of the string with length 0, i.e., the bare hole as zero in energy and denoting ν as the length of the string—i.e., the number of shifted spins—the eigenvalue is

$$E_\nu=\frac{J}{2}(2\nu+1). \tag{1}$$

This is exact for $\nu\leq 2$ and is true for "most" longer strings as well. For simplicity we assume Eq. (1) to be true for any

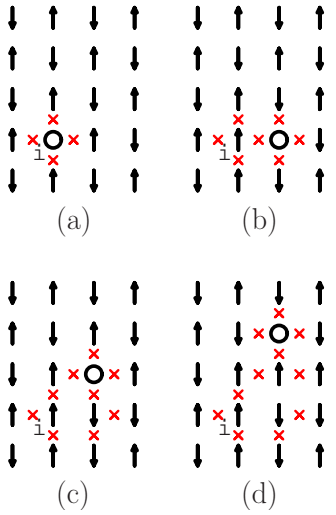

FIG. 1. (Color online) The mechanism of the string effect. Slanted crosses represent links with the contribution to the Ising part of the exchange energy higher by $J/2$ as compared to the Néel state. (b) A string state obtained by a single move of the hole created at site i. [(c) and (d)] States obtained, respectively, by two and three consecutive moves.

string. This implies that the hole is trapped in a linearly ascending potential and all eigenstates of H_0 are localized. The main deviations from Eq. (1) occur for "loops" as discussed by Trugman[4] which, in fact, lead to hole propagation even in the t-J_z model. Such loops pose no fundamental problem for the present formalism and can be dealt with by introducing the concept of "irreducible paths" as discussed in detail in Ref. 40.

Next we note that by acting with a point-group operation, which leaves the initial site i invariant, the string states $|\mathcal{P}_i\rangle$ are transformed into one another. We can therefore define linear combinations of the $|\mathcal{P}_i\rangle$ which transform like the basis states of the irreducible representations of C_{4v} under these point-group operations. Then we make the following ansatz for a localized eigenstate of H_0:

$$|\Psi_i^{(o,m)}\rangle = \sum_{\mathcal{P}_i} \alpha_{\mathcal{P}_i}^{(o,m)} |\mathcal{P}_i\rangle, \tag{2}$$

where $o \in \{s, p_x, p_y, d_{x^2-y^2}, d_{xy}, \cdots\}$ denotes the symmetry or "orbital character" of the state and m labels the excitation number for a given symmetry. In keeping with Eq. (1) we moreover assume that each coefficient $\alpha_{\mathcal{P}_i}^{(o,m)}$ can be factorized into a sign $\phi_{\mathcal{P}_i}^{(o)}$—which plays the role of an "angular wave function"—and a "radial-wave function" $\alpha_\nu^{(o,m)}$ which depends only on the length of the string,

$$\alpha_{\mathcal{P}_i}^{(o,m)} = \phi_{\mathcal{P}_i} \alpha_\nu^{(o,m)}. \tag{3}$$

For an A_1 (s-wave) state the sign $\phi_{\mathcal{P}_i}$ is obviously uniform for all paths. For an E (p-wave) or B_1 ($d_{x^2-y^2}$-wave) state $\phi_{\mathcal{P}_i}$ is determined by the direction of the first hop away from the site i as shown in Fig. 2. The string of length 0, i.e., the bare hole at site i, is invariant under all point-group operations and hence has nonvanishing weight only in the s-like state—this implies that E and B_1 states are higher in energy than the

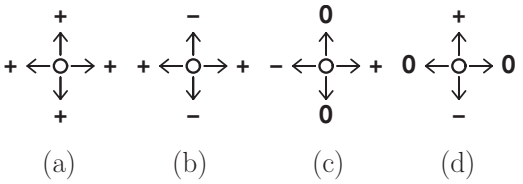

FIG. 2. Dependence of the sign of a given path on the direction of the first move for the (b) $d_{x^2-y^2}$-wave SP, (c)p_x-wave SP, and (d) p_y-wave SP. (a) For completeness the schematic representation for the s-wave SP has also been shown.

A_1 state because they are composed of strings with length ≥ 1 and hence a minimum of three frustrated bonds. For the two remaining representations A_2 (g wave) and B_2 (d_{xy} wave) it can be shown that only strings with a minimum length of 2 have nonvanishing weight in the corresponding SP states—these states therefore are even higher in energy and we omit them. For each symmetry sector o we can now set up the Schrödinger equation,

$$H_0 |\Psi_i^{(o,m)}\rangle = E^{(o,m)} |\Psi_i^{(o,m)}\rangle, \tag{4}$$

thereby assuming Eq. (1) and solving for the eigenenergies $E^{(o,m)}$ and the coefficients α—this is explained in Appendix A. As expected for a linearly ascending potential, the α's are rapidly decreasing with increasing length of the string even for the physical parameter range $t/J \approx 3$. It turns out the Schrödinger equation for the coefficients α for the $d_{x^2-y^2}$ SP is identical to that for the p-like ones. To shorten the notation we call the coefficients $\alpha_\nu^{(s,0)}$ for the lowest s-like SP α_ν and instead of those for the p-like SP, $\alpha_\nu^{(p,0)}$, and d_{x2-y2}-like SP, $\alpha_\nu^{(d,0)}$, we use $\alpha'_\nu/\sqrt{2}$ and $\alpha'_\nu/2$, respectively.

III. EFFECTIVE MULTIBAND MODEL FOR SPIN POLARONS

So far we have found SP states [Eq. (2)] which form a set of approximate localized eigenstates of H_0 at each of the sites of the sublattice A. Next we note that the remaining part H_1 of the tJM—which comprises the transverse part of the Heisenberg exchange and the hopping terms $\propto t', t''$—has nonvanishing matrix elements between SP states centered on neighboring sites i and j. One important mechanism leading to such a matrix element is the truncation of the string shown in Fig. 3. By flipping the first two spins of the defect string the starting point of the string is shifted to a second or third nearest neighbor while the length of the string is reduced by 2. Since the coefficients $\alpha_{\mathcal{P}_i}^{(o,m)}$ and $\alpha_{\mathcal{P}'_j}^{(o')}$ of the initial and final strings are known by solution of Eq. (4) and the strength of the spin-flip term is $J/2$, the corresponding matrix element is easily evaluated. Similarly, the hopping terms $\propto t', t''$ allow for the hopping of the bare hole between the sites of one sublattice (see Fig. 3). In addition there is the "loop hopping"[4] and actually a wide variety of additional processes, which are discussed in Appendix A.

Assuming that the matrix elements are known we define Fourier transforms,

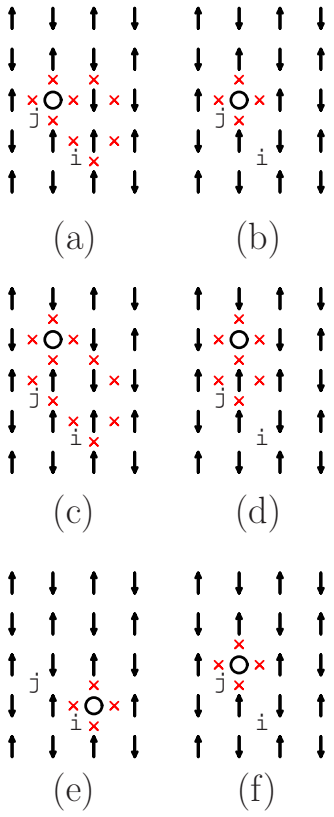

FIG. 3. (Color online) (a)→(b): a string of length 2 starting at i is truncated to a string of length 0 at j by the transverse part of the Heisenberg exchange. (c)→(d): a string of length 3 is reduced to one of length 1. (e)→(f): a bare hole at site i (string of length 0) is transported to j by t' hopping.

$$|\Psi^{(\lambda)}(\mathbf{k})\rangle = \sqrt{\frac{2}{N}} \sum_{j\in A} |\Psi_j^{(\lambda)}\rangle e^{-i\mathbf{k}\cdot\mathbf{R}_j}, \tag{5}$$

where $\lambda=(o,m)$. Next we make the linear combination of atomic orbitals (LCAO)-like ansatz for a propagating single-hole state,

$$|\Phi_l(\mathbf{k})\rangle = \sum_{\lambda} v_{\lambda}^{(l)}(\mathbf{k}) |\Psi^{(\lambda)}(\mathbf{k})\rangle, \tag{6}$$

which leads to a generalized eigenvalue problem of the form

$$H_{\mathrm{eff}}(\mathbf{k})\mathbf{v}_l(\mathbf{k}) = E_l(\mathbf{k})\mathrm{O}_{\mathrm{eff}}(\mathbf{k})\mathbf{v}_l(\mathbf{k}), \tag{7}$$

where the Hamilton and overlap matrices are given by

$$H_{(\lambda\lambda')} = \delta_{\lambda\lambda'}E^{(\lambda)} + \mathcal{T}^{(\lambda\lambda')}(\mathbf{k}), \tag{8}$$

$$O_{(\lambda\lambda')} = \delta_{\lambda\lambda'} + \mathcal{O}^{(\lambda\lambda')}(\mathbf{k}), \tag{9}$$

and we have introduced the Fourier transform of

$$\mathcal{T}_{ii'}^{(\lambda\lambda')} = \langle\Psi_i^{(\lambda)}|H_1|\Psi_{i'}^{(\lambda')}\rangle, \tag{10}$$

$$\mathcal{O}_{ii'}^{(\lambda\lambda')} = \langle\Psi_i^{(\lambda)}|\Psi_{i'}^{(\lambda')}\rangle. \tag{11}$$

All these matrix elements can be expressed in terms of the coefficients $\alpha_l^{(\lambda)}$ as discussed in Appendix A. Once these matrix elements are calculated we readily obtain the band structure for the spin polarons.

To conclude this section we briefly discuss the relationship with previous work. Several authors have studied hole motion in an antiferromagnet by calculations within a string basis.[4,45–47] The difference is that the diagonalization of H_0 leads to a considerable reduction in basis states in that high lying eigenstate of H_0 that are eliminated from the very beginning. The matrices to be diagonalized in the present work are 4×4 or 10×10—which is very small compared to the matrix dimensions in Refs. 4 and 45–48. Moreover the LCAO-like scheme makes it easier to extract a physical picture. Another frequently applied approach is the self-consistent Born approximation.[7–12,49–51] The single-hole wave function associated with this approximation actually can also be interpreted as a superposition of string states once the Fourier-transformed version of the wave function in Ref. 54 is converted into real space. This explains why the results, e.g., for the dispersion of a single hole are practically identical.

IV. PHOTOEMISSION SPECTRA AND FERMI SURFACE

ARPES gives the information on the one-electron removal part of the spectral function defined, at $T=0$, as

$$A^{-}(\mathbf{k},\omega) = -\frac{1}{\pi}\mathrm{Im}\langle\Psi_{\mathrm{AF}}|c_{\mathbf{k},\downarrow}^{\dagger}\frac{1}{\omega - H + i0^{+}}c_{\mathbf{k},\downarrow}|\Psi_{\mathrm{AF}}\rangle. \tag{12}$$

$|\Psi_{\mathrm{AF}}\rangle$ in Eq. (12) represents the half-filled ground state in which the photoemission process takes place. This approach is based on the so-called three-step model of photoemission.[52] A more sophisticated approach based on the single-step model[53] is beyond the scope of this paper. Since we assume that the rigid-band scenario is applicable to cuprates in the low doping range, we expect that the conclusions drawn from that analysis are also to some extent applicable to doped systems.

As a first step we approximate the resolvent operator $(\omega - H + i0^{+})^{-1}$ by

$$\frac{1}{\omega - H + i0^{+}} \to \sum_{l,\mathbf{k}} \frac{|\Phi_l(\mathbf{k})\rangle\langle\Phi_l(\mathbf{k})|}{\omega - E_l(\mathbf{k}) + i0^{+}}, \tag{13}$$

i.e., we restrict the single-hole states to the coherent superposition of SP states [Eq. (6)]. Next, we have to choose an approximate ground state $|\Psi_{\mathrm{AF}}\rangle$ of the Heisenberg antiferromagnet. The simplest choice would be the Néel state $|\Phi_N\rangle$ but in this way we would miss an important mechanism for a $\mathbf{k}$-dependent quasiparticle weight, namely, the coupling of the photohole to quantum spin fluctuations. By generating a hole in the Néel state we can obtain only a bare hole, i.e., the string of length 0. In the presence of quantum spin fluctuations the photoemission process can also generate strings of length 1 or 2 (see Fig. 4). Since in such a process the hole is created not at the central site i of the SP state—which determines the phase factor $e^{-i\mathbf{k}\cdot\mathbf{R}_i}$ in the Bloch state [Eq. (5)]—the photoemission matrix element becomes $\mathbf{k}$ dependent. Generally speaking the fact that the SP quasiparticles extend over more than one unit cell in real space results in a "struc-

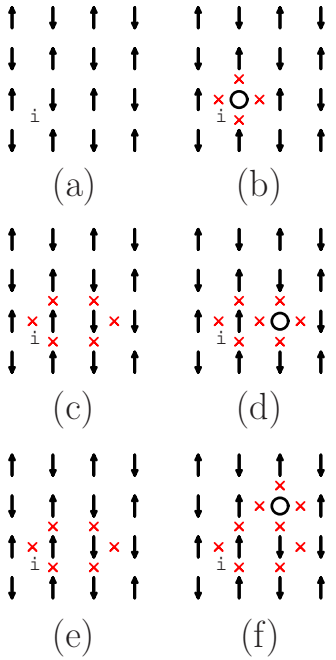

FIG. 4. (Color online) (a)→(b): creation of a bare hole at site i from the Néel state. (c)→(d): creation of a string of length 1 starting at i from the Néel state+quantum fluctuation. (e)→(f): creation of a string of length 2 starting at i from the Néel state+quantum fluctuation.

ture factor" which varies within the first Brillouin zone in $\mathbf{k}$ space. As will be seen below, this very $\mathbf{k}$ dependence is the source of the remnant Fermi surface. In order to capture this effect we use simple first-order perturbation theory for the quantum spin fluctuations and set

$$|\Psi_{\mathrm{AF}}\rangle = |\Phi_N\rangle - \frac{1}{3}\sum_{\langle i,j\rangle}(S_i^+ S_j^- + \mathrm{H.c.})|\Phi_N\rangle. \tag{14}$$

Since second-order perturbation theory gives quite a good estimate for the ground-state energy of the Heisenberg antiferromagnet, we expect that the probability for coupling to a quantum fluctuation with the electron annihilation operator is described quite well by Eq. (14).

Since a quantum fluctuation in the initial states simply gives rise to an extra factor of $-1/3$ we immediately obtain the following expressions for the photoemission matrix element $m^{(\lambda)}=\langle\Psi_{\downarrow}^{(\lambda)}(\mathbf{k})|c_{\mathbf{k},\downarrow}|\Psi_{\mathrm{AF}}\rangle$:

$$m^{(s)}(\mathbf{k}) = \alpha_0 - \frac{2\alpha_1}{3}[\cos(k_x)+\cos(k_y)] - \frac{4\alpha_2}{3}\{[\cos(k_x)+\cos(k_y)]2-1\},$$

$$m^{(p_x)}(\mathbf{k}) = \frac{\sqrt{2}i\alpha_1'}{3}\sin(k_x) + \frac{2\sqrt{2}i\alpha_2'}{3}\sin(k_x)[\cos(k_x)+\cos(k_y)],$$

$$m^{(d)}(\mathbf{k}) = -\frac{\alpha_1'}{3}[\cos(k_x)-\cos(k_y)] - \frac{\alpha_2'}{3}[\cos 2(k_x)-\cos 2(k_y)]. \tag{15}$$

Using these matrix elements we can now compute the spectral density from the normalized SP eigenfunctions.

If we want to compare to experiment, however, there is yet another important effect we need to take into account, namely, the coupling of the photohole to charge fluctuations. We may expect that the ground state of the system has not only quantum spin fluctuations but also charge fluctuations, i.e., an admixture of pairs of holes and double occupancies with a density $\propto(t/U)^2$. By annihilating an electron on a doubly occupied site it is possible to create a string state with an initial site i by annihilating an electron at a site different from i. Again, this will give rise to a $\mathbf{k}$ dependence of the spectral weight. Such processes actually are not described by the tJM, but since it is rather easy to discuss them we do so. We treat the charge fluctuations in perturbation theory, i.e., we replace

$$|\Psi_{\mathrm{AF}}\rangle \to |\Psi_{\mathrm{AF}}\rangle + \frac{t}{U}\sum_{\langle ij\rangle}\sum_{\sigma}\hat{d}_{i\sigma}^{\dagger}\hat{c}_{j\sigma}|\Phi_N\rangle, \tag{16}$$

where $\hat{d}_{i\sigma}^{\dagger}=c_{i\sigma}^{\dagger}n_{i\bar{\sigma}}$. The hopping terms $\propto t',t''$ do not produce charge fluctuations in the Néel state. Denoting $\eta=t/U=J/(4t)$ we get the following correction to the matrix element $m^{(s)}$:

$$m^{(s)}(\mathbf{k}) = 2\eta\alpha_0[\cos(k_x)+\cos(k_y)] - 4\eta\alpha_1, \tag{17}$$

whereas the corrections to $m^{(p_x)}$ and $m^{(d)}$ are zero. It might appear that the corrections due to charge fluctuations are quite small, being anyway $\propto t/U$. On the other hand, by coupling to charge fluctuations a bare hole at site i can be created by actually annihilating an electron on any of its z neighbors. By changing from $\mathbf{k}=(0,0)$ to $\mathbf{k}=(\pi,\pi)$ the corresponding contribution to the photoemission matrix element thus changes from zt/U to $-zt/U$ and since this has to be added before squaring the matrix element the impact of the charge fluctuations is, in fact, quite strong. The way in which we are treating charge fluctuations would be adequate for a simple one-band Hubbard model, which is not the proper model for cuprate superconductors. A very similar calculation for the more correct two-band model has been done by Eroles *et al.*[55]

In a first calculation we want to study the low-energy-band structure. In the LCAO-like ansatz (6) we first restrict ourselves to the lowest state (i.e., $m=1$) for each symmetry o so that we have to solve 4×4 matrices (we have $o\in\{s,p_x,p_y,d_{x^2-y^2}\}$). The resulting band structure is shown in Fig. 5. Using the photoemission matrix elements [Eq. (15)] the photoemission spectrum can be calculated (see Fig. 6). In addition to the familiar quasiparticle band discovered in $Sr_2CuO_2Cl_2$ by Wells *et al.*,[3] which has been discussed extensively in the literature,[5–12,38,39] there is a second band with slightly lower intensity which has predominant p-like SP character and runs essentially parallel to the original band.

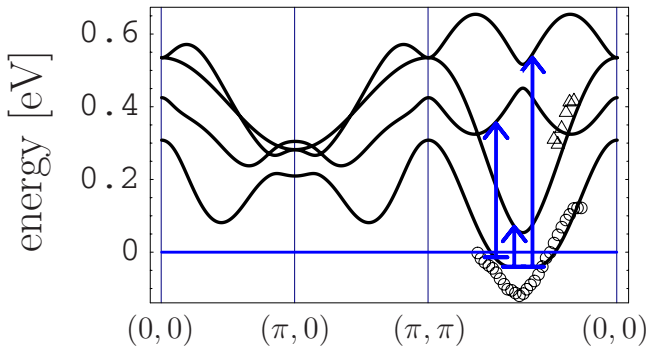

FIG. 5. (Color online) Band structure obtained by solving the eigenvalue problem [Eq. (7)]. Also shown is the dispersion of bands observed by Ronning *et al.* (Ref. 57) in $Ca_2CuO_2Cl_2$ (circles and triangles). A sample Fermi level of a doped system has been chosen as the zero of energy. Vertical arrows label possible optical transitions of a hole at the bottom of the band.

Indeed such a second band with weaker intensity which follows the main band is seen in exact diagonalization of small clusters (see, e.g., Fig. 1 of Ref 17). These higher lying SP bands have small spectral weight and therefore could be hard to observe in ARPES—even more so because the ARPES spectra in the undoped compound are likely to show strong lattice polaronic effects.[56] Nevertheless, it may be that a higher lying band—possibly the first *p*-like band—has been observed by Ronning *et al.*[57] in the insulating cuprate $Ca_2CuO_2Cl_2$. There a second weak band has been observed at roughly 0.5 eV below the quasiparticle band. Ronning *et al.*[57] interpreted this as part of a wide band which reaches Γ at a binding energy below 2 eV. As can be seen in Fig. 5, however, this band (triangles) has a dispersion that is quite comparable to that of the quasiparticle band (circles). Moreover, as will be discussed below, we believe that the band portion observed in $Ca_2CuO_2Cl_2$ around Γ at binding energies around 2 eV is an example of a "1 eV peak" as observed in $Sr_2CuO_2Cl_2$ (Ref. 58) and thus unrelated to the band marked by triangles. While the higher lying bands may be hard to observe in ARPES optical interband transitions between the main band and these higher lying bands produce finite-frequency optical conductivity which may correspond to the mid-IR bands, again in the actual compounds this may be complicated by polaronic effects. Another feature which can be seen in Fig. 6 and which is quite consistent with experiment is the sharp drop of the spectral weight of the quasiparticle band which occurs whenever one passes (roughly) through the Fermi surface of the noninteracting half-filled, i.e., the remnant Fermi surface. It is caused by the **k** dependence of the photoemission matrix elements [Eqs. (15) and (17)] and therefore reflects the interplay of spin and charge fluctuations in the spin background and the internal structure of the quasiparticle. Assuming that the structure of the quasiparticles remains roughly the same in a spin background without long-range order but short-ranged antiferromagnetic correlations—as is suggested by exact diagonalization[32]—the **k** dependence of the photoemission matrix element should be similar for finite doping. This would provide an immediate explanation for the Fermi arcs seen in the underdoped compounds. To make this more quantitative we have computed the Fermi contour by filling up the single-hole dispersion according to the Pauli principle—see Fig. 5—and showed it in the upper panel of Fig. 7. The lower panel shows the spectral weight of the quasiparticle band as a function of the Fermi-surface angle. The hole pocket is actually more elongated along the (1,1) direction than along the antiferromagnetic zone boundary. It should be noted, however, that this is calculated at half-filling where $(\pi,0)$ is far from the valence-band top due to the t' and t'' terms (see Fig. 5). On the other hand it is known that upon doping the band portions near $(\pi,0)$ move upward.[13] It has been suggested that decreasing antiferromagnetic spin correlations leads to an effective downward renormalization of t' and t'' with doping[17] so that for finite doping the pocket is probably elongated more along the antiferromagnetic zone boundary as observed by Chang *et al.*[20] This effect cannot be reproduced by our simple theory, however. Another phenomenon which would find a very simple explanation in an approximate rigid-band behavior upon doping is the pseudogap.[13] The upper part of Fig. 8 shows again the hole pocket and a contour in **k** space which extends the "front part" of the pocket into a free-electron-like Fermi surface. The pseudogap is usually defined by measuring the leading-edge shift or the dispersion of the high-energy feature along such a contour. The lower part of Fig. 8 then shows the energy of the quasiparticle band along this "Fermi surface" plotted versus the Fermi-surface angle Φ. There is the characteristic flat part near $\phi=0$ which originates because the contour initially follows the hole pocket and then the *d*-wave-like downward dispersion as the free-electron-like Fermi surface departs

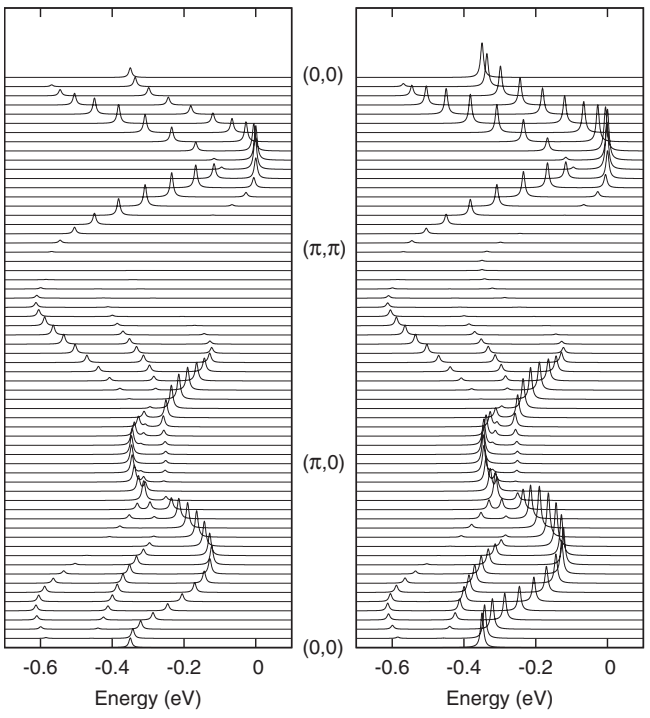

FIG. 6. Photoemission spectrum for the half-filled model corresponding to the band structure [Eq. (5)]. In the left panel the spectral weight is computed using only the quantum fluctuation correction [Eq. (15)]; in the right panel the charge-fluctuation correction [Eq. (17)] was used as well.

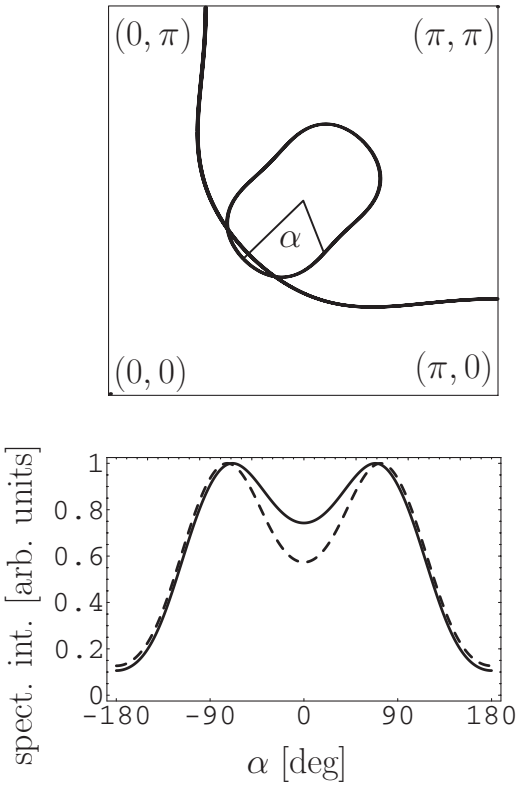

FIG. 7. Top: Fermi surface obtained for 10% hole concentration by rigid filling of the lowest SP band. Bottom: spectral weight of the corresponding SP band along the Fermi surface as a function of the angle α.

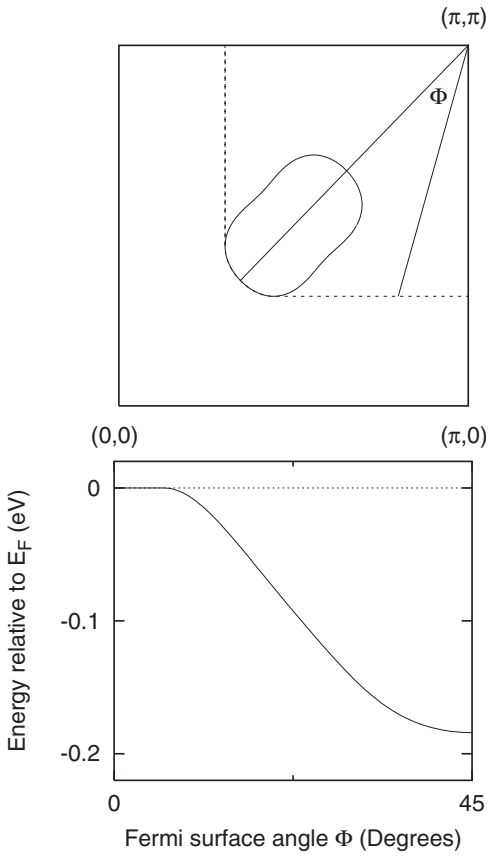

FIG. 8. Top: Fermi surface obtained for 10% hole concentration by rigid filling of the lowest SP band and a contour obtained by extending the "inner part" of the pocket to a free-electron-like Fermi surface. Bottom: energy relative to Fermi energy of the SP band forming the pocket along the free-electron-like Fermi surface as a function of Fermi-surface angle.

from the hole pocket. It should be noted that this would explain only the high-energy pseudogap. On the other hand the low-energy pseudogap, being defined in terms of a leading-edge shift, has no immediate connection with a dispersion relation and will almost certainly depend also on the temperature and momentum dependent linewidth of the quasiparticle band.[18] In fact, assuming a lifetime broadening $\Gamma(\mathbf{k}) \propto |E(\mathbf{k}) - \mu|$ would immediately explain also the low-energy pseudogap. As noted above the pocket in Fig. 8 is too much elongated in (1,1) direction. However, the effective downward renormalization of t' and t'' in the doped compounds would lead to a pocket that is more elongated along the magnetic zone boundary. In any way, however, if one would go along the inner part of the pocket near (1,1) and extend this to a free-electron-like Fermi surface as in the top part of Fig. 8, one will always see a dispersion as shown in the bottom part of Fig. 8.

Finally we want to discuss the spectral function on a larger energy scale. To keep the discussion simple we keep only *s*-like SP states in Eq. (6) but include excited *s*-like states with $m=1, \ldots, 10$ (extending this to $m=1, \ldots, 20$ produces no visible change in the spectra—this is one of the beneficial effects of the "prediagonalization" of H_0). Moreover we retain only the matrix elements due to string truncation and the t' and t'' terms, i.e., processes of the type shown in Fig. 3. However, we do include the full photoemission matrix elements [Eqs. (15) and (17)]. The resulting spectral function is shown in Fig. 9. In addition to the quasiparticle band—which is essentially identical to the one of the more exact calculation shown in Fig. 6 above—there now appear additional bands at higher energy. In reality these "bands" probably are not well-defined states because they are already high in energy. Rather these states are probably strongly broadened due to interaction with magnons and phonons and may have only the character of "resonances." Whereas the quasiparticle band is composed mainly of the lowest *s*-like SP states for motion of the hole trapped in the linearly ascending potential, the higher lying bands correspond to excited levels of the trapped hole. The relatively high intensity of these states may be understood by noting that the coefficients $\alpha_\nu^{(m)}$ for the excited states $m>1$ will have extra nodes as functions of ν and if the signs of the $\alpha_\nu^{(m)}$ better match the prefactors in Eq. (15) the matrix element may even be larger for these higher lying states.

The spectral function in Fig. 9 is qualitatively similar to the result of a recent calculation by Bonča *et al.*[47] which was performed in a string basis with several million basis states. As already noted the main difference between the present calculation and the one by Bonča *et al.*[47] is in the fact that the prediagonalization of H_0 by solution of Eq. (4) leads to a quite massive reduction in irrelevant degrees of freedom in the present scheme—as noted above, the matrix diagonalized

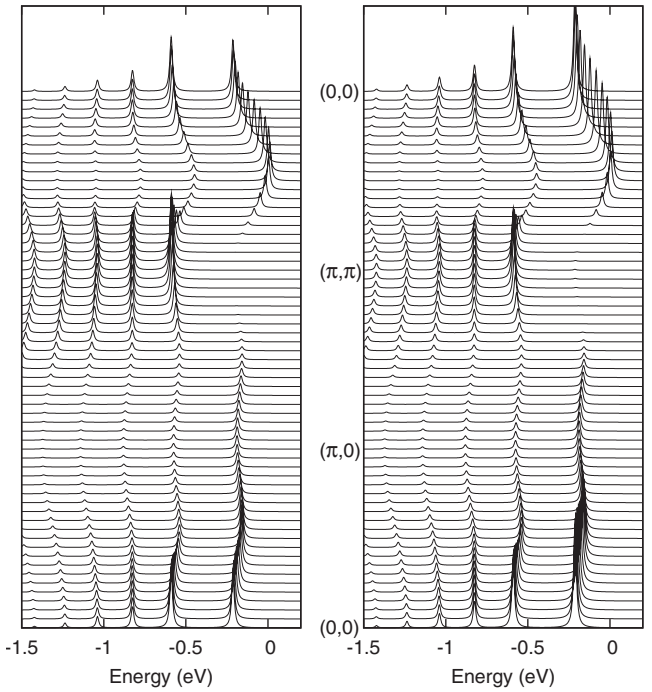

FIG. 9. Spectral density for hole creation at half-filling along high-symmetry lines in the Brillouin zone. Calculated with (right) and without (left) the contribution from charge fluctuations.

here is 10×10. Despite this simplification not only the dispersion of the topmost peak but also the fact that the high-energy part "widens" as one moves away from (0,0) is reproduced. On the other hand, it should also be noted that the spectral weight shown in Fig. 9 cannot directly be compared with Ref. 47 because we are taking into account the corrections of the ARPES matrix element due to quantum spin fluctuations in the half-filled ground state which are not included there.

V. ELECTRONIC STRUCTURE AT HIGHER BINDING ENERGIES

Recently a number of studies have revealed additional structure in the ARPES spectra at higher binding energies. Ronning *et al.*[57] found that in the insulating cuprate $Ca_2CuO_2Cl_2$ the quasiparticle band seems to "fade away" as the Γ point is approached—a phenomenon which is common to all cuprates. The spectral weight that is missing from the quasiparticle band then appears at ≈1.5 eV below the maximum of the quasiparticle band in the form a high-intensity band which has a dispersion that is remarkably consistent with local-density approximation (LDA) band-structure calculations. More precisely this is the antibonding band of Cu $3d_{x^2-y^2}$ and O $2p\sigma$ orbitals—whereby it has to be kept in mind that at Γ these two orbitals do not hybridize due to parity, so that in an LCAO-like description these bands have pure oxygen character at Γ and—by continuity in $\mathbf{k}$—very small Cu $3d$ admixture its neighborhood.

Similar behavior was observed in doped cuprates as well.[59–63] In addition, the so-called waterfall phenomenon is observed. Moving, e.g., along the (1,1) direction toward Γ the quasiparticle band first disperses away from the Fermi edge but then—at a momentum of approximately $(\frac{\pi}{4},\frac{\pi}{4})$—seems to bend down sharply and drop almost vertically down to an energy of ≈1 eV below the Fermi edge. The apparent vertical part of the dispersion—the "waterfalls"—can be seen as a hump in momentum distribution curves at binding energies in the range of 0.5 $\rightarrow$1.0 eV. Upon reaching ≈1 eV below E_F the vertical parts then merge with two LDA-like bands of high intensity.

Similar behavior—namely, small band portions with a free-electron-like dispersion and high spectral weight near high-symmetry points of the Brillouin zone—has been observed previously in the insulating compound $Sr_2CuO_2Cl_2$ by Pothuizen *et al.*[58] The interpretation given by these authors was that these are O $2p$ derived states which do not hybridize with Cu $3d$ orbitals due to symmetry—which is why they appear only at high-symmetry points of the Brillouin zone—and hence are unaffected by the strong correlations in the partially filled Cu $3d$ orbitals. This explains their LDA-like dispersion and high spectral weight because they are essentially free-electron states.

We believe that an important clue to the interpretation of the waterfalls is the finding of Inosov *et al.*[64] who showed that matrix element effects play a crucial role in their observation and that the missing part of the quasiparticle band near Γ can, in fact, be observed with photon energies around 100 eV where the cross section for Cu $3d$ orbitals becomes appreciable.[65] Moreover, Pan *et al.*[62] found that the waterfalls show the same dependence on photon polarization as the quasiparticle band itself, indicating that they are also derived from Zhang-Rice singlets (ZRSs). Moreover finally in our opinion the crucial clue is the fact that the quasiparticle band itself cannot be observed near the Γ point either. While numerical studies of the Hubbard and t-J model[66–68]—as well as the present theory—do indeed predict that the spectral weight of this band is lower by a factor of 2–3 at Γ as compared to $(\frac{\pi}{2},\frac{\pi}{2})$, in experiment there is practically no more intensity visible. Rather, the spectra show a complete suppression of spectral weight around Γ which extends down to the intense LDA-like bands. Most significantly, however, the waterfalls appear at very nearly the same momentum where the quasiparticle band itself becomes visible.

We conclude that the reason for the vanishing of the quasiparticle band near Γ is "extrinsic" to the t-J or single-band Hubbard model, namely, the special combination of phases for the O $2p\sigma$ orbitals in the bonding combination which hybridizes with a given Cu $3d_{x^2-y^2}$ orbital in the ZRS. In the framework of a simple three-step model of photoemission for photoemission the effect that we seek comes from the matrix element for the dipole transition from O $2p$ states into the final state—which we take to be a plane wave with momentum $\mathbf{k}$ for simplicity. For definiteness we introduce the dipole matrix element,

$$\epsilon\cdot\mathbf{v}_\alpha=\frac{1}{\sqrt{V}}\int d\mathbf{r}e^{-i\mathbf{k}\cdot\mathbf{r}}\epsilon\cdot\mathbf{r}\psi_\alpha(\mathbf{r}), \tag{18}$$

where ϵ denotes the polarization vector of the light, V is the volume of the crystal, and $\psi_\alpha(\mathbf{r})$ is the wave function of an

O $2p$ orbital at the origin and $\alpha \in \{x,y\}$. The matrix element for a dipole transition from the bonding combination of O $2p\sigma$ oxygen orbitals around a given Cu site j,

$$P_{j,\sigma} = \frac{1}{2}(p_{j+\hat{x}/2,\sigma} - p_{j-\hat{x}/2,\sigma} - p_{j+\hat{y}/2,\sigma} + p_{j-\hat{y}/2,\sigma}), \quad (19)$$

into the plane-wave state is

$$m_{\mathrm{ZRS}} = e^{-i\mathbf{k}\cdot R_j} i\left[\mathbf{v}_y \sin\left(\frac{k_y}{2}\right) - \mathbf{v}_x \sin\left(\frac{k_x}{2}\right)\right] \cdot \boldsymbol{\epsilon}. \quad (20)$$

Note that the $\mathbf{k}$ dependence of the expression in square brackets comes solely from the interplay between the phase factors $e^{i\mathbf{k}\cdot\mathbf{r}}$ on the four oxygen neighbors of atom j and the relative phases of the orbitals in Eq. (19). Namely, any two oxygen orbitals whose position in real space differs by one lattice spacing have a relative phase of (-1) in the ZRS—which would correspond to momentum (π,π). This $\mathbf{k}$ dependence is therefore completely independent of details in the computation of the matrix elements $\mathbf{v}_\alpha$ and therefore in particular independent of the photon polarization. Moreover it would stay the same if a more realistic final-state wave function was used as long as this is a Bloch state with momentum $\mathbf{k}$. It now can be seen that $m_{\mathrm{ZRS}} \to 0$ as $\mathbf{k} \to (2n\pi, 2m\pi)$. Unlike the argument based on the dipole selection rule which was discussed by Ronning *et al.*[57] expression (20) thus explains why the quasiparticle band has vanishing intensity not only at Γ but also at all equivalent points in higher Brillouin zones as well.

The above considerations apply only to hole creation on oxygen. For photon energies around 20 eV it is well known, however, that the cross section for hole creation on oxygen is considerably larger than for hole creation in transition-metal $3d$ orbitals.[65] Moreover, starting from a d^9 state one would reach a d^8 state. The latter is high in energy and hence has small weight in the ZRS and moreover the resulting spectral weight would be spread over several eV due to the multiplet splitting of d^8 so that the corresponding matrix element certainly is small. A d^9 final state could be produced by photoemission from d^{10} state but this state also is high in energy and therefore has small weight in the ground state. In any way the contribution of hole creation on Cu is strongly suppressed. For larger photon energies—around 100 eV—Inosov *et al.*[64] could indeed resolve the quasiparticle band but only at $(2\pi,0)$. Obviously the larger photoemission cross section and the nonvalidity of the dipole selection rule at this momentum make it possible to see intensity from photoholes in Cu $3d_{x^2-y^2}$ orbitals. Clear evidence that the intensity seen there is due to photohole creation on Cu is also provided by the strong variation of intensity around the Cu $3p \to$ Cu $3d$ threshold which is being used routinely to identify transition-metal $3d$ states in other transition-metal oxides.[69]

One might then ask where the spectral weight corresponding to hole creation on oxygen goes at Γ. The answer is that this spectral weight is concentrated in the LDA-like bands which are observed around the Γ point at approximately 1.5 eV below the Fermi energy. Due to parity the "antibonding band" of Cu $3d_{x^2-y^2}$ and O $2p\sigma$ orbitals actually has pure oxygen character at Γ. If a Bloch state of O $2p$ orbitals is created with momentum (0,0) this cannot couple to the ZRS singlet [see Eq. (20)] but has overlap 1 with these bandlike states. This is the same reasoning as given by Pothuizen *et al.*[58] for the 1 eV peaks in $Sr_2CuO_2Cl_2$. The spectral weight transfer from the quasiparticle band to the 1 eV peaks at Γ as observed by Ronning *et al.*[57] thus is strong evidence for the ZRS character of the quasiparticle band.

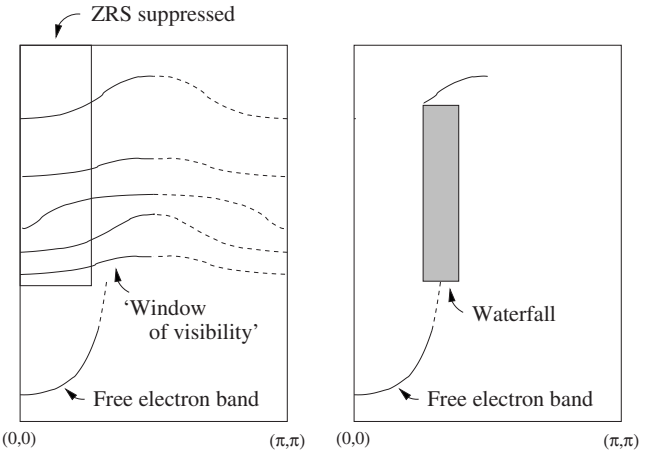

FIG. 10. Interpretation of the waterfall phenomenon. Around Γ photoholes on oxygen do not couple to the ZRS whence all t-J derived states have no spectral weight. Photoholes created with this momentum on oxygen instead propagate as (nearly) free-electron states which do not hybridize with the correlated Cu d orbitals. Moving away from Γ the t-J bands become visible but lose spectral weight as well (dashed potions). The nearly free-electron states cease to exist because they now have appreciable hybridization with the correlated Cu d orbitals. The higher lying SP bands thus are visible only in a small window in $\mathbf{k}$ space, i.e., the waterfalls.

These leave the question as to what is the interpretation of the waterfalls. The above considerations suggest that these are simply the higher lying SP bands seen in Fig. 9. These bands are likely to be strongly broadened due to interaction with spin excitations and possible also phonons although one of them may have been resolved by Ronning *et al.*[57] (see Fig. 5). Near Γ the spectral weight of these bands disappears because they are also "t-J derived" and the matrix element for creation of a ZRS vanishes (see Fig. 10). As one moves away from Γ the matrix element for creation of a ZRS increases but—as can be seen in Fig. 9—the spectral weight of these excited SP bands now quickly decreases. It follows that the spectral weight of these bands must go through a maximum as one moves away from Γ and this is our interpretation of the waterfalls: a number of essentially incoherent states which have a "window of visibility" in a narrow range of momenta around $(\frac{\pi}{4},\frac{\pi}{4})$ and this window of visibility is seen as the hump in the momentum distribution curves. Since the suppression of these states near Γ is governed by the same matrix element of the ZRS as the quasiparticle band itself, it is moreover clear that this window of visibility "opens" precisely in the same range of $\mathbf{k}$ where the quasiparticle band itself becomes visible—hence the apparent downward bending and the waterfall-like appearance of the spectra.

A more quantitative description of this phenomenon obviously would have to start out from a three-band model so as

to describe both the coupling of a photohole to a ZRS and the existence of the nearly free-electron states at high-symmetry points. This is out of the scope of the present paper and we therefore make no attempt for a quantitative discussion. There have been a number of attempts to explain the waterfall phenomenon within the t-J model.[51,70] However, as was already noted, the experimental spectra show a complete suppression of spectral weight around Γ which extends downward all the way to the intense LDA-like bands. This behavior is not reproduced by t-J model calculations which show spectral weight—corresponding to the higher lying bands in Fig. 9—at too low binding energy. Moreover, the LDA-like dispersion of the high-intensity parts near Γ is not really reproduced

VI. OPTICAL CONDUCTIVITY

Finally we turn to a discussion of the optical conductivity thereby using the results of the simplified calculation which took into account only the lowest $(m=1)$ state for each symmetry o. As is the case for atomic wave functions the s- and d-like SP states on one hand and the p-like SP states on the other have opposite parity and hence can have nonvanishing matrix elements of the current operator in between them. If we assume again that the quasiparticle band is filled with holes upon doping—which would occupy momenta around $(\frac{\pi}{2},\frac{\pi}{2})$—we thus expect optical interband transitions (as indicated in Fig. 5) which should be observable in the finite-frequency optical response. This is defined as

$$\sigma_\delta(\mathbf{q}=0,\omega)=\sum_{n\neq 0}\frac{1}{\omega}|\langle\psi_n|j_\delta(\mathbf{q}=0)|\psi_0\rangle|^2\delta[\omega-(E_n-E_0)],$$

where $|\psi_n\rangle$ (E_n) denotes the nth eigenstate (eigenenergy) of the system (in particular, $n=0$ denotes the ground state). Also, j_δ with $\delta=x,y$ denotes a component of the current operator,

$$\mathbf{j}(\mathbf{q})=i\sum_{m,n}t_{mn}e^{i\mathbf{q}\cdot(\mathbf{R}_m+\mathbf{R}_n)/2}[\mathbf{R}_m-\mathbf{R}_n]\hat{c}^\dagger_{m,\sigma}\hat{c}_{n,\sigma}. \quad (21)$$

Assuming a filling of the quasiparticle band we approximate this by

$$\sigma_\delta(\omega)=2\sum_{\mathbf{k}}\sum_{l=1}^{3}\frac{1}{\omega}|\langle\Phi_l(\mathbf{k})|j_\delta|\Phi_1(\mathbf{k})\rangle|^2 n_{\mathbf{k}} \times\delta\{\omega-[E_l(\mathbf{k})-E_1(\mathbf{k})]\}, \quad (22)$$

where $n_{\mathbf{k}}$ denotes the hole occupation of the quasiparticle $(l=1)$ band. To evaluate this we need matrix elements of the current operator between the localized SP states [Eq. (2)]: $\langle\Psi_i^\lambda|j_\delta|\Psi_i^{\lambda'}\rangle$ [with $\lambda=(o,m)$]. The main contributions to this matrix element are shown in Fig. 11. Starting from a bare hole—the "string of length 0"—the current operator j_y generates two strings of length 1 but with opposite sign. These two string states thus have precisely the right sign to couple to a p_y-like SP state (see the sign convention in Fig. 2). From this and similar processes we obtain the matrix element,

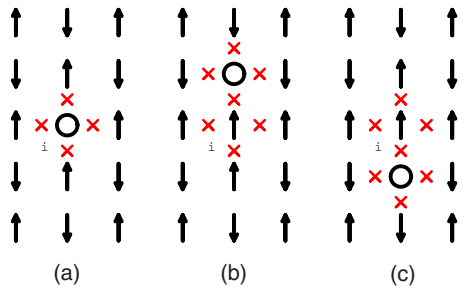

FIG. 11. (Color online) Application of the current operator j_y to a bare hole in the Néel state (a) creates two strings of length 1 [(b) and (c)] with opposite signs.

$$\langle\Psi_i^{(p_\delta 0)}|j_\delta|\Psi_i^{(s),0}\rangle=2i\left(\sum_{\mu=0}\alpha_\mu\alpha'_{\mu+1}-\sum_{\mu=1}\alpha'_\mu\alpha_{\mu+1}\right). \quad (23)$$

All matrix elements generated in a similar way and involving SPs of different symmetries or hopping at longer distances have been listed in Appendix B. The resulting optical conductivity at a hole concentration of 10% is shown in Fig. 12. While the higher lying bands with p character have small spectral weight and hence are difficult to observe in ARPES, they dominate the optical conductivity. We note that the present interpretation of the optical conductivity is consistent with that of Refs. 34 and 43. One may expect that the excited levels of the trapped hole—or "internal degrees of freedom" of the SP quasiparticles—are also seen in the dynamical density correlation function. Vojta and Becker[34] calculated the dynamical density correlation function in a string framework similar to the one used by Bonča *et al.*[47] and obtained convincing agreement with exact diagonalization results. Within our approach one can naturally explain the distribution and spreading of the spectral intensity over a wide energy range, which has been observed in experiments.[71,72] Due to the Brillouin folding in the AF state the center of the hole pocket at $(\pi/2,\pi/2)$ is a high-symmetry point. s, d, and p SP states do not mix with each other exactly at this point. Thus, the transitions with similar intensity occur in the weakly doped system between the lowest predominantly s like and the first and the third predominantly p-like bands. Wider spreading of the high-intensity region at higher energies can be attributed to the admixture of p-wave SPs to the lowest band and transition to the predominantly d-wave second excited band.

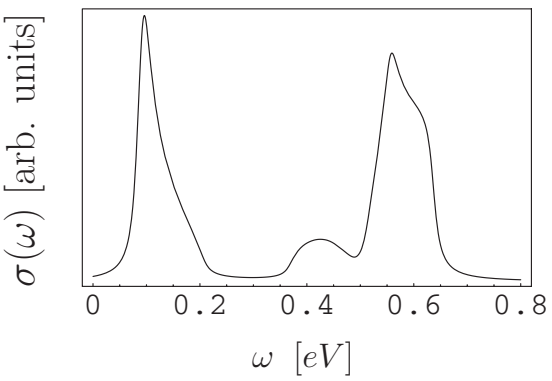

FIG. 12. Optical conductivity at 10% hole concentration.

VII. DISCUSSION AND CONCLUSIONS

In summary we have presented a theory for spin-polaron-like quasiparticles. The basic idea is that a hole in an antiferromagnetically ordered "spin background" is self-trapped which actually requires only short-range antiferromagnetic order. This will lead to a hierarchy of localized states which may also realize different irreducible representations of C_{4v}. Since the Heisenberg exchange and the t' and t'' terms have matrix elements between such self-trapped states on neighboring sites an LCAO-like description emerges where the role of the atomic or Wannier functions is played by the levels of the self-trapped hole. This leads to a multiband structure for the doped holes with the lowest of these being the familiar quasiparticle band observed in the insulating compounds and discussed extensively in the literature. Here we take the point of view that the simplest description for the underdoped compounds is holes being filled into this quasiparticle band. The fact that these self-trapped states extend over several unit cells in real space necessarily implies that they have an ARPES form factor which varies within the first Brillouin zone—hence the strong variation of the photoemission intensity of the quasiparticle band as a function of $\mathbf{k}$ which explains the remnant Fermi surface and the Fermi arcs seen in ARPES. Moreover, the pseudogap becomes a triviality within this picture. One of the higher bands of the effective LCAO Hamiltonian may have been observed in ARPES in the insulator $Ca_2CuO_2Cl_2$ and optical transitions between the resulting bands may explain the mid-infrared band in optical spectroscopy. There are probably complications due to lattice polaron effects but here we neglect these although the simplicity of the present calculation—which never need matrices to more than 10×10—would certainly allow to treat such effects as well.

The main drawback of the present theory is the use of a spin background with antiferromagnetic order—which clearly is not realized in doped materials of interest. On the other hand all processes by which the hole propagates involve only spins in its immediate neighborhood. One may therefore expect that very similar processes would occur in a spin background with only short-range antiferromagnetic correlations so that much of the present theory should apply in this case as well. The most important effect we are missing with the present calculation is the closing of the pseudogap with both increasing temperature and increasing doping. Since this closing implies that the dispersion actually approaches that for the "pure" t-J model—i.e., without t' and t'' terms—this effect could be described by an effective downward renormalization of the t' and t'' terms. The mechanism may be the decrease in spin correlations: in the Néel state the t' and t'' terms can transport a hole "completely coherent," i.e., without creating a spin excitation. As the spin-correlation length decreases and reaches the "range" of these terms in real space—two lattice spacings—the t' and t'' will increasingly generate spin excitations when transporting a hole so that they change their net effect from coherent hole transport to "excitation generating" hole transport.

ACKNOWLEDGMENTS

P.W. acknowledges encouragement and valuable comments from P. Fulde and R. Micnas. He also appreciates discussions with M. Jarrel, P. Prelovšek, and T. Tohyama.

APPENDIX A: SPIN-POLARON MODEL

We first derive the equations for the coefficients $\alpha^{(o,m)}(l)$ in Eq. (2), thereby assuming Eq. (3). We denote by $|\Phi_\nu\rangle$ the sum of all string states with ν inverted spins, each multiplied by the proper phase factors according in Fig. 2. On a Bethe lattice the number of such states is $n_\nu=f^{(o)}z(z-1)^{\nu-1}$, where $f^{(o)}=1$ for $o=s,d_{x^2-y^2}$ and $f^{(o)}=1/2$ for $o=p_x,p_y$. Our normalized basis states are $|\nu\rangle=n_\nu^{-1/2}|\Phi_\nu\rangle$ which obey

$$\langle \nu+1|H_t|\nu\rangle = t\sqrt{\frac{n_{\nu+1}}{n_\nu}}$$

because each of the $n_{\nu+1}$ basis string states in the bra is generated exactly once from a state in the ket and the matrix element for hopping of a hole is positive. The states [Eq. (2)] can be written as

$$|\Psi_i\rangle = \sum_\nu \beta_\nu|\nu\rangle,$$

with $\beta_\nu=n_\nu^{1/2}\alpha_\nu^{(o,m)}$. Performing the variational procedure—thereby using Eq. (1)—we obtain the following set of equations:

$$E_0\beta_0+\sqrt{z}t\beta_1=E\beta_0, \tag{A1}$$

$$E_1\beta_1+\sqrt{z}t\beta_0+\sqrt{z-1}t\beta_2=E\beta_1, \tag{A2}$$

$$E_\nu\beta_\nu+\sqrt{z-1}t(\beta_{\nu-1}+\beta_{\nu+1})=E\beta_\nu. \tag{A3}$$

For $o=p_x,p_y,d_{x^2-y^2}$ one has to set $\beta_0=0$ and discard the first equation. After introducing a cutoff for ν these equations can be solved numerically.

Now we proceed to analyze with some sample processes which give rise to nonvanishing matrix elements [Eqs. (10) and (11)]. The hopping integral t is the highest energy scale among all model parameters t, t', t'', and J. On the other hand, the exchange energy grows fast with the number of fluctuations. That number is directly related to the length of paths $\mathcal{P}_i$. This mechanism is responsible for the tendency toward hole confinement and the construction of SPs also relies on it. Quasiparticle deconfinement occurs due to processes which are mediated by hopping to second and third NN and by the action of the XY term in the exchange interaction. Only string states $|\mathcal{P}_i\rangle$ with low number fluctuations can be involved in those processes at the low-energy scale. Thus, in order to find matrix elements [Eq. (10)] we need to determine coupling between short-string states $|\mathcal{P}_i\rangle$. That coupling is induced by the perturbation part H_1 which by definition contains terms related to hopping to second and third NN sites and which also contains the XY term. We restrict our considerations to processes involving string states $|\mathcal{P}_i\rangle$ which are related to paths not longer than two lattice spacings for s-wave SPs and to paths not longer than three lattice spacings for SPs with lower symmetry. In the latter case we take into account longer strings because the zero-

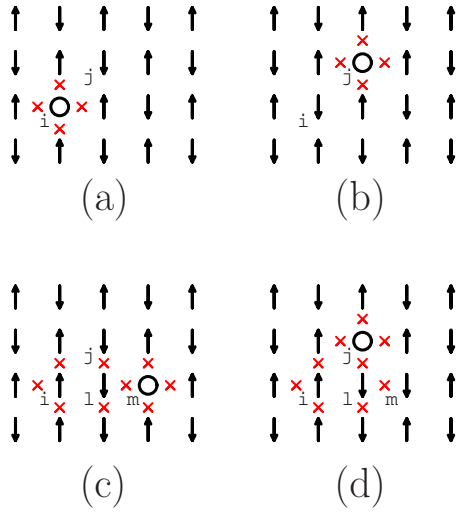

FIG. 13. (Color online) [(a) and (b)] A process which gives rise to the shift of the s-wave SP to a second NN site. [(c) and (d)] A process which generates corrections to eigenenergies E_1 and E_1' of SPs.

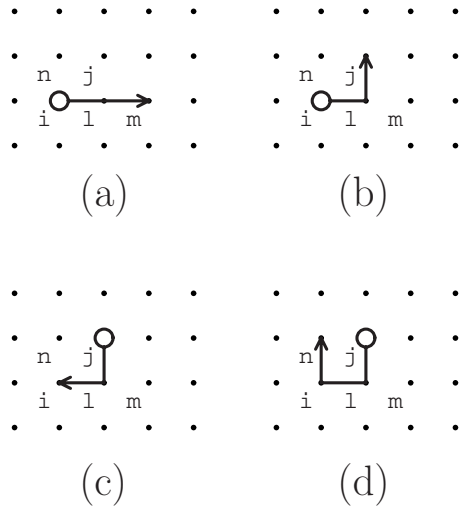

FIG. 14. [(a) and (b)] A different representation of string states depicted in Figs. 13(c) and 13(d), respectively. (c) A string state contributing to a process which involves hopping to second NN sites. That process gives rise to SP shifts along plaquette diagonals. (d) A string state contributing to a process which involves hopping to NN sites.

length string state $|\mathcal{P}_i\rangle$ does not contribute to the wave function [Eq. (2)] of SPs with lower symmetry and thus the weight is shifted to states representing longer paths. The absolute values of prefactors α_μ and α_μ' corresponding to lowest eigenstates of Eqs. (A1)–(A3) rapidly decrease with the string length μ which additionally justifies the restriction of our considerations to strings with short length. At the level of the approximation which we apply, there exist more than 20 categories of processes which contribute to Eqs. (10) and (11). The differences between different categories concern the underlying mechanisms or the geometry of involved strings. Since the mechanisms which give rise to coupling between s-wave SPs were discussed in detail in the past,[40,44] here we will mainly concentrate on the issue how the lowering of SP symmetry influences the coupling between SPs and we will discuss representative examples of processes which give rise to the hybridization between SPs. In order to keep the Hilbert space as small as possible we consider at first the low-energy sector and analyze only lowest SP states with given symmetry.

For example, Figs. 13(a) and 13(b) depict a process during which a SP polaron is shifted to a second NN site. (a) represents a string state $|\mathcal{P}_i\rangle$ which is a component of the wave function (2) of a SP created at site i. This state has been obtained by creating a bare hole in the Néel state. It appears with the prefactor α_0 in superposition (2) defining the s-wave SP at site i. With the same prefactor appears the string state depicted in Fig. 13(b). It is a component of the s-wave SP created at site j. Since string states (a) and (b) are coupled by the second NN hopping term a nonvanishing matrix element [Eq. (10)] between s-wave SPs is generated. The related contribution to that matrix element is given by

$$\delta T_{ji}^{[(s,0)(s,0)]} \equiv \delta T_{\mathbf{R}_j-\mathbf{R}_i}^{(ss)} = \tau_{ss}^{(1)} = t' \alpha_0^2. \tag{A4}$$

Within a convention for presenting matrix elements this contribution can be written as

$$ss, \hat{\mathbf{x}} + \hat{\mathbf{y}}, \tau_{ss}^{(1)}: C_4. \tag{A5}$$

The presence of the group symbol C_4 in Eq. (A5) means that additional contributions to Eq. (10) can obtained by applying to Eq. (A4) elements of C_4 different than identity. Since $\alpha_0' \equiv 0$ states depicted in Figs. 13(a) and 13(b) do not contribute to SP wave functions [Eq. (2)] with lower symmetry. Thus the above discussed lowest-order process does not generate hybridization in which such SPs are involved. By process order we understand, in terms of the conventional perturbation theory, the total number of Hamiltonian actions necessary to transform a state representing a bare hole created in the AF background into another such state. It is clear that this parameter is related to the sum of lengths for paths involved in a given process.

The origin of the formula for the integral $\tau_{ss}^{(1)}$ in Eq. (A4) is rather obvious. It is the product of prefactors which appear by string states depicted in Figs. 13(a) and 13(b) in the definition for the wave functions of SPs at sites i and j. t' is the integral which appears as a prefactor in the hopping term coupling those string states. The same scheme can be applied to deduce the form of hopping integrals which appear in further terms in $\mathcal{T}_{\mathbf{R}}^{(oo')}$.

Figures 13(c) and 13(d) depict a process which gives rise to corrections to SP eigenenergies E_1 and E_1' of SPs and amendments to the diagonal term in Eq. (8). Those corrections originate with the coupling between different string states generated by the hopping to second NN sites. Those string states contribute to the wave functions of SPs created at the site i. The paths $\mathcal{P}_i$ corresponding to string states $\mathcal{P}_i$ depicted in Figs. 13(b) and 13(c) have been shown in Figs. 14(a) and 14(b), respectively. From now on we will also use the latter form of diagrams to represent string states. The same mechanism as discussed above works for pairs of

longer strings which have identical forms with the exception of hole positions at ends of them. The corrections to energies of s-wave, d-wave, and p-wave SPs are $\tau_{ss}^{(13)}$, $\tau_{dd}^{(13)}$, and $\tau_{pp}^{(13)}$, respectively. Their explicit form can be found below. Due to point-group properties the above discussed process does not generate the coupling between SPs with different symmetries.

During another process which also involves strings of length two lattice spacings the action of hopping to second NN sites generates shifts of SPs between second NN sites. Surprisingly, SPs are shifted now in the direction opposite to the direction of the bare hole move. The nature of that paradox can be understood by analyzing Figs. 14(b) and 14(c). The action of the second NN hoping term on the string state [Fig. 14(b)], which contributes to the SP created at site i, shifts the hole at the end of that string from site j to site i and generates a string state [Fig. 14(c)], which contributes to the SP created at site j. That process gives rise to a new contribution to $\mathcal{T}_{\mathbf{R}}^{(oo')}$,

$$ss,\hat{\mathbf{x}}+\hat{\mathbf{y}},\tau_{ss}^{(15)};dd,\hat{\mathbf{x}}+\hat{\mathbf{y}},\tau_{dd}^{(15)},$$

$$p_y p_x,\hat{\mathbf{x}}+\hat{\mathbf{y}},\tau_{pp}^{(15)}:C_{4v}, \tag{A6}$$

$$p_y s,\hat{\mathbf{x}}+\hat{\mathbf{y}},\tau_{ps}^{(15)};p_y d,\hat{\mathbf{x}}+\hat{\mathbf{y}},\tau_{pd}^{(15)}:C_{4v}\cdot \mathrm{H.c.} \tag{A7}$$

The presence of the group symbol C_{4v} means as before that contributions (A6) and (A7) should be supplemented by matrix elements obtained by applying to the existing elements all group elements and in the case of the second line also elements obtained by applying the Hermitian conjugation. The process depicted in Figs. 14(b) and 14(c) gives rise to the hybridization of SPs with different symmetries because apart from the case of coupling between s-wave and d-wave SPs no selection rule forbids it and also because string states depicted in both Figs. 14(b) and 14(c) can be components of wave functions for SPs of arbitrary symmetry. The hopping integrals $\tau_{oo'}^{(15)}$ as usually are given by products of the bare hopping integral t' and of prefactors with which string states depicted in Figs. 14(b) and 14(c) appear in the definition of SPs. The existence of negative signs in some of integrals $\tau_{oo'}^{(15)}$ originates with the fact that due to symmetry properties of some SPs such signs are also contained in prefactors of string states in sums [Eq. (2)] defining those SPs.

After discussing some representative examples of SP coupling generated by hopping to second NN sites we skip the discussion of analogous processes mediated by hopping to third NN sites, because their mechanisms are similar, and analyze a high-order process which involves hopping to NN sites. That process has been neglected during the construction SPs because a long-string state participates in it. The NN hopping operator, by shifting the hole at the end of the string depicted in Fig. 14(d) from site n to site j, generates the string state depicted in Fig. 14(b), which gives rise to a new contribution to the coupling between SPs created at sites i and j. For the sake of clarity, we only additionally mention briefly that Fig. 14(d) represents a string state in which flipped spins occupy sites j, l, and i and the hole occupies site n. It is clear that the same mechanism generates the hopping of SPs between all second NN sites. Depending on the symmetry of the initial and final SP states, related hopping integrals are given by $\tau_{sd}^{(21)}$, $\tau_{dd}^{(21)}$, $\tau_{pd}^{(21)}$, $\tau_{sp}^{(21)}$, and $\tau_{pp}^{(21)}$.

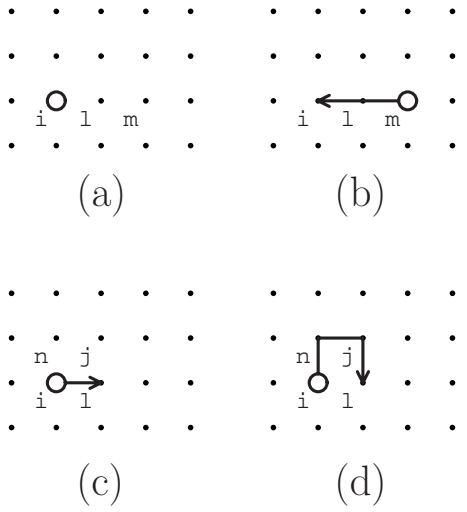

FIG. 15. [(a) and (b)] A low-order process which involves the action of the transverse part of the exchange term and gives rise to the hybridization of SPs with different symmetry. [(c) and (d)] String states involved in a process mediated by the XY part of the exchange term and resulting in a correction to the eigenenergy of the d-wave SP.

The analysis of Hamiltonian terms induced by the exchange interaction can be performed along similar lines. We start with a necessary correction to the Ising part of the exchange energy. When we have been constructing the Schrödinger equations [Eqs. (A1)–(A3)] for wave functions [Eq. (2)] of SPs, we have assumed that the Ising contribution depends on the length of strings but does not depend on their geometry. That assumption is true for short strings, but for longer strings there exists some exceptions from that rule. For example, by inspecting the spin structure of the string state depicted Fig. 14(d), we see that one broken bond has been saved for that state in comparison with strings which have the same length and have the starting and ending points which are not NNs. That fact gives rise to the decrease by $J/2$ of the string-state energy and to corrections to eigenenergies of d-wave and p-wave SPs. Those corrections are given by $\iota_{dd}^{(19)}$ and $\iota_{pp}^{(19)}$, respectively. Since the amendments are related to strings of length at least three lattice spacings we neglect them in the case of the s-wave SP because the weight of related string states in the wave function of the s-wave SP is small.

Also the best known in literature process which determines to great extent the overall shape of the single-particle energy dispersion at the low-energy scale gives rise to the hybridization between SPs with different symmetries. That process has been shown in Figs. 15(a) and 15(b). Flipping spins at sites l and m in the string state depicted in Fig. 15(a) by the transverse part of the exchange energy gives rise to the string state depicted in Fig. 15(b) and to the hybridization between SPs at sites i and m. In that kind of hybridization the s-wave state should be involved because the state shown in Fig. 15(a) represents a bare hole created in the Néel state. As

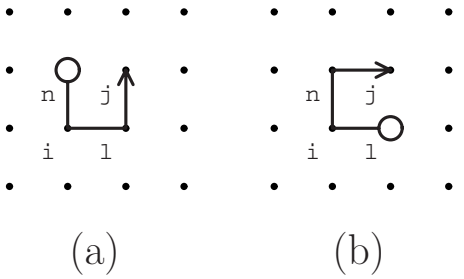

FIG. 16. [(a) and (b)] Spuriously different string states which are actually identical, which gives rise to the overlap between SPs created at sites n and l.

we have shown before, such string states do not contribute to wave functions of SPs with lower symmetry. The hopping integrals which appear at terms coupling an s-wave SP with an s-wave, a d-wave, and a p-wave SP located at a third NN site are given by $\iota_{ss}^{(3)}$, $\iota_{ds}^{(3)}$, and $\iota_{ps}^{(3)}$, respectively.

A similar mechanism gives rise to a correction to the eigenenergy of a d-wave SP. The action of the XY term flips spins in the string state depicted in Fig. 15(c) at sites n, j and creates the string state shown in Fig. 15(d). Due to the fact that both string states contribute to the wave functions [Eq. (2)] of SPs created at the same site i and due to standard selection rules, the contribution to $\mathcal{T}_{\mathbf{R}}^{(oo')}$ originating with the above discussed process must be diagonal. For this reason, p-wave states cannot contribute to the related new matrix elements $\mathcal{T}_{\mathbf{R}}^{(oo')}$ because the process depicted in Figs. 15(c) and 15(d) involves string states which contribute to different p_x-wave and p_y-wave SPs. Since the length of the string depicted in Fig. 15(d) is three lattice spacings we neglect the correction to the eigenenergy of the s-wave SP because we expect that it is small. The correction to the eigenenergy of the d-wave SP is $-\iota_{dd}^{(11)}$. It also contains contributions related to the coupling, in the same way, between longer-string states obtained by letting holes at the ends of strings in Figs. 15(c) and 15(d) to hop further along identical paths.

During the construction of SPs we have been assuming that wave functions of SPs at different sites are orthogonal which turns out not to be an exactly true assumption. On the other hand the overlap between SPs is rather small because it originates with the overlap of nominally different string states related with paths of relatively long length. Such string states have been depicted in Figs. 16(a) and 16(b). Both Figs. 16(a) and 16(b) actually represent the same state which consists of a hole at site j and fluctuations at sites n, i, and l created in the Néel state. The generated in this way overlap between different SPs also gives rise to a new contribution in the Hamilton operator,

$$p_y d,\hat{\mathbf{x}}+\hat{\mathbf{y}},E_1'\omega_{pd}^{(1)}:C_{4v}\cdot \mathrm{H.c}\,., \tag{A8}$$

$$dd,\hat{\mathbf{x}}+\hat{\mathbf{y}},E_1'\omega_{dd}^{(1)};p_y p_x,\hat{\mathbf{x}}+\hat{\mathbf{y}},E_1'\omega_{pp}^{(1)}:C_{4v}. \tag{A9}$$

The analysis of other processes which give rise to new elements of $\mathcal{T}_{\mathbf{R}}^{(oo')}$ is rather straightforward and similar to the analysis of previously discussed processes. Thus we do not discuss the remaining contributions to $\mathcal{T}_{\mathbf{R}}^{(oo')}$ one by one.

Finally, we list here matrix elements which determine the form of the Hamilton matrix [Eqs. (8) and (10)],

$$ss,0,E_1;dd,0,E_1';p_x p_x,0,E_1';p_y p_y,0,E_1', \tag{A10}$$

$$ss,0,\tau_{ss}^{(6)};ss,\hat{\mathbf{x}}+\hat{\mathbf{y}},\tau_{ss}^{(1)};ss,2\hat{\mathbf{x}},\chi_{ss;(2,0)}^{(\beta)},$$

$$dd,0,\tau_{dd}^{(6)};dd,2\hat{\mathbf{x}},\tau_{dd}^{(14)};p_x p_x,0,\tau_{pp}^{(6)},$$

$$p_x p_x,2\hat{\mathbf{x}},\tau_{pp}^{(14)}:C_4, \tag{A11}$$

$$ss,00,\tau_{ss}^{(13)};ss,2\hat{\mathbf{x}},\iota_{ss}^{(3)};ds,2\hat{\mathbf{x}},\chi_{ds;(2,0)}^{(\gamma)},$$

$$dd,0,\tau_{dd}^{(13)};dd,2\hat{\mathbf{x}},\iota_{dd}^{(7)};dp_x,2\hat{\mathbf{x}},\iota_{dp}^{(7)},$$

$$p_x s,2\hat{\mathbf{x}},\chi_{p_x s;(2,0)}^{(\gamma)};p_x d,2\hat{\mathbf{x}},\chi_{p_x d;(2,0)}^{(\gamma)},$$

$$p_x p_x,0,\tau_{pp}^{(13)};p_x p_x,2\hat{\mathbf{x}},\iota_{pp}^{(7)}:C_4\cdot \mathrm{H.c}\,., \tag{A12}$$

$$ss,\hat{\mathbf{x}}+\hat{\mathbf{y}},\iota_{ss}^{(3)};sd,\hat{\mathbf{x}}+\hat{\mathbf{y}},\tau_{sd}^{(21)},$$

$$sp_x,\hat{\mathbf{x}}+\hat{\mathbf{y}},\tau_{sp}^{(21)};dd,\hat{\mathbf{x}}+\hat{\mathbf{y}},\chi_{dd;(1,1)}^{(\delta)},$$

$$dd,0,-\iota_{dd}^{(11)};dd,2\hat{\mathbf{x}},-\iota_{dd}^{(7)},$$

$$dp_x,\hat{\mathbf{x}}+\hat{\mathbf{y}},\chi_{dp_x;(1,1)}^{(\delta)};p_x d,\hat{\mathbf{x}}+\hat{\mathbf{y}},\chi_{p_x d;(1,1)}^{(\delta)},$$

$$p_x d,2\hat{\mathbf{x}},\iota_{pd}^{(7)};p_x p_x,\hat{\mathbf{x}}+\hat{\mathbf{y}},\chi_{p_x p_x;(1,1)}^{(\delta)},$$

$$p_y s,\hat{\mathbf{x}}+\hat{\mathbf{y}},\chi_{p_y s;(1,1)}^{(\delta)};p_y d,\hat{\mathbf{x}}+\hat{\mathbf{y}},\chi_{p_y d;(1,1)}^{(\delta)},$$

$$p_y p_x,\hat{\mathbf{x}}+\hat{\mathbf{y}},\chi_{p_y p_x;(1,1)}^{(\delta)}:C_{4v}\cdot \mathrm{H.c}\,., \tag{A13}$$

$$ss,0,\chi_{ss;(0,0)}^{(\epsilon)};ss,\hat{\mathbf{x}}+\hat{\mathbf{y}},\tau_{ss}^{(15)},$$

$$dd,0,\chi_{dd;(0,0)}^{(\epsilon)};dd,\hat{\mathbf{x}}+\hat{\mathbf{y}},\chi_{dd;(1,1)}^{(\epsilon)},$$

$$p_x p_x,0,\chi_{p_x p_x;(0,0)}^{(\epsilon)};p_x p_x,\hat{\mathbf{x}}+\hat{\mathbf{y}},\tau_{pp}^{(23)},$$

$$p_y p_x,\hat{\mathbf{x}}+\hat{\mathbf{y}},\chi_{p_y p_x;(1,1)}^{(\epsilon)}:C_{4v}, \tag{A14}$$

$$p_y p_x,\hat{\mathbf{x}}+\hat{\mathbf{y}},\tau_{pp}^{(21)}:C_{2v}\cdot \mathrm{H.c.} \tag{A15}$$

and of the overlap matrix [Eqs. (9) and (11)],

$$p_y d,\hat{\mathbf{x}}+\hat{\mathbf{y}},\omega_{pd}^{(1)}:C_{4v}\cdot \mathrm{H.c}\,., \tag{A16}$$

$$dd,\hat{\mathbf{x}}+\hat{\mathbf{y}},\omega_{dd}^{(1)};p_y p_x,\hat{\mathbf{x}}+\hat{\mathbf{y}},\omega_{pp}^{(1)}:C_{4v}, \tag{A17}$$

where

$$\chi_{ss;(2,0)}^{(\beta)}=\tau_{ss}^{(2)}+\tau_{ss}^{(14)}, \tag{A18}$$

$$\chi_{ds;(2,0)}^{(\gamma)}=\iota_{ds}^{(3)}+\tau_{ds}^{(14)}, \tag{A19}$$

$$\chi^{(\gamma)}_{p_x s;(2,0)} = \iota^{(3)}_{ps} + \tau^{(14)}_{ps}, \tag{A20}$$

$$\chi^{(\gamma)}_{p_x d;(2,0)} = \iota^{(7)}_{pd} + \tau^{(14)}_{pd}, \tag{A21}$$

$$\chi^{(\delta)}_{dd;(1,1)} = \iota^{(11)}_{dd} + \tau^{(17)}_{dd} + \tau^{(18)}_{dd}, \tag{A22}$$

$$\chi^{(\delta)}_{dp_x;(1,1)} = \iota^{(7)}_{pd} - \iota^{(11)}_{pd} + \tau^{(17)}_{pd} + \tau^{(18)}_{pd}, \tag{A23}$$

$$\chi^{(\delta)}_{p_x d;(1,1)} = \iota^{(7)}_{pd} + \iota^{(11)}_{pd} + \tau^{(23)}_{pd}, \tag{A24}$$

$$\chi^{(\delta)}_{p_x p_x;(1,1)} = \iota^{(7)}_{pp} + \iota^{(11)}_{pp}, \tag{A25}$$

$$\chi^{(\delta)}_{p_y s;(1,1)} = \iota^{(3)}_{ps} + \tau^{(15)}_{ps}, \tag{A26}$$

$$\chi^{(\delta)}_{p_y d;(1,1)} = \iota^{(7)}_{pd} + \tau^{(15)}_{pd} + \tau^{(17)}_{pd} + \tau^{(18)}_{pd} + (E_1' - J/2)\omega^{(1)}_{pd} + \tau^{(21)}_{pd}, \tag{A27}$$

$$\chi^{(\delta)}_{p_y p_x;(1,1)} = \iota^{(7)}_{pp} + \tau^{(17)}_{pp} + \tau^{(18)}_{pp}, \tag{A28}$$

$$\chi^{(\epsilon)}_{ss;(0,0)} = \tau^{(5)}_{ss} + \tau^{(16)}_{ss}, \tag{A29}$$

$$\chi^{(\epsilon)}_{dd;(0,0)} = \tau^{(5)}_{dd} + \tau^{(16)}_{dd} + \iota^{(19)}_{dd} + \tau^{(22)}_{dd}, \tag{A30}$$

$$\chi^{(\epsilon)}_{dd;(1,1)} = \tau^{(15)}_{dd} + (E_1' - J/2)\omega^{(1)}_{dd} + \tau^{(21)}_{dd} - \tau^{(22)}_{dd}, \tag{A31}$$

$$\chi^{(\epsilon)}_{p_x p_x;(0,0)} = \tau^{(16)}_{pp} + \tau^{(19)}_{pp}, \tag{A32}$$

$$\chi^{(\epsilon)}_{p_y p_x;(1,1)} = \tau^{(15)}_{pp} + (E_1' - J/2)\omega^{(1)}_{pp}, \tag{A33}$$

$$\tau^{(1)}_{ss} = t'\alpha_0^2, \tag{A34}$$

$$\tau^{(2)}_{ss} = t''\alpha_0^2, \tag{A35}$$

$$\iota^{(3)}_{ss} = \frac{J}{2}\sum_{\mu=0} 3^{\mu}\alpha_\mu\alpha_{\mu+2},$$

$$\iota^{(3)}_{ds} = \frac{J}{4}\sum_{\mu=0} 3^{\mu}\alpha_\mu\alpha'_{\mu+2},$$

$$\iota^{(3)}_{ps} = -\frac{J}{2\sqrt{2}}\sum_{\mu=0} 3^{\mu}\alpha_\mu\alpha'_{\mu+2}, \tag{A36}$$

$$\tau^{(5)}_{ss} = t'\alpha_1^2, \tau^{(5)}_{dd} = -\frac{t'}{4}(\alpha_1')^2, \tag{A37}$$

$$\tau^{(6)}_{ss} = t''\alpha_1^2, \tau^{(6)}_{dd} = \frac{t''}{4}(\alpha_1')^2,$$

$$\tau^{(6)}_{pp} = -\frac{t''}{2}(\alpha_1')^2, \tag{A38}$$

$$\iota^{(7)}_{dd} = \frac{J}{8}\sum_{\mu=1} 3^{\mu-1}\alpha'_\mu\alpha'_{\mu+2},$$

$$\iota^{(7)}_{pd} = -\frac{J}{4\sqrt{2}}\sum_{\mu=1} 3^{\mu-1}\alpha'_\mu\alpha'_{\mu+2},$$

$$\iota^{(7)}_{pp} = \frac{J}{4}\sum_{\mu=1} 3^{\mu-1}\alpha'_\mu\alpha'_{\mu+2}, \tag{A39}$$

$$\iota^{(11)}_{dd} = \frac{J}{8}\left[\alpha_1'\alpha_3' + 2\sum_{\mu=2} 3^{\mu-2}\alpha'_\mu\alpha'_{\mu+2}\right],$$

$$\iota^{(11)}_{pd} = -\frac{J}{4\sqrt{2}}\left[\alpha_1'\alpha_3' + 2\sum_{\mu=2} 3^{\mu-2}\alpha'_\mu\alpha'_{\mu+2}\right],$$

$$\iota^{(11)}_{pp} = -\frac{J}{4}\left[\alpha_1'\alpha_3' + 2\sum_{\mu=2} 3^{\mu-2}\alpha'_\mu\alpha'_{\mu+2}\right], \tag{A40}$$

$$\tau^{(13)}_{ss} = 2t'\sum_{\mu=2} 3^{\mu-2}\alpha_\mu^2, \tau^{(13)}_{dd} = \frac{t'}{2}\sum_{\mu=2} 3^{\mu-2}(\alpha'_\mu)^2,$$

$$\tau^{(13)}_{pp} = t'\sum_{\mu=2} 3^{\mu-2}(\alpha'_\mu)^2, \tag{A41}$$

$$\tau^{(14)}_{ss} = t''\alpha_2^2, \tau^{(14)}_{ds} = \frac{t''}{2}\alpha_2\alpha_2',$$

$$\tau^{(14)}_{ps} = -\frac{t}{\sqrt{2}}\alpha_2\alpha_2', \tau^{(14)}_{dd} = \frac{t''}{4}(\alpha_2')^2,$$

$$\tau^{(14)}_{pd} = -\frac{t''}{2\sqrt{2}}(\alpha_2')^2, \tau^{(14)}_{pp} = -\frac{t''}{2}(\alpha_2')^2, \tag{A42}$$

$$\tau^{(15)}_{ss} = t'\alpha_2^2, \tau^{(15)}_{ps} = -\frac{t'}{\sqrt{2}}\alpha_2\alpha_2',$$

$$\tau^{(15)}_{dd} = -\frac{t''}{4}(\alpha_2')^2, \tau^{(15)}_{pd} = -\frac{t'}{2\sqrt{2}}(\alpha_2')^2,$$

$$\tau^{(15)}_{pp} = -\frac{t'}{2}(\alpha_2')^2, \tag{A43}$$

$$\tau^{(16)}_{ss} = t''\sum_{\mu=2} 3^{\mu-2}\alpha_\mu^2, \tau^{(16)}_{dd} = \frac{t''}{4}\sum_{\mu=2} 3^{\mu-2}(\alpha'_\mu)^2,$$

$$\tau^{(16)}_{pp} = \frac{t''}{2}\sum_{\mu=2} 3^{\mu-2}(\alpha'_\mu)^2, \tag{A44}$$

$$\tau^{(17)}_{dd} = -\frac{t''}{4}(\alpha_3')^2, \tau^{(17)}_{pd} = -\frac{t''}{2\sqrt{2}}(\alpha_3')^2,$$

$$\tau_{pp}^{(17)} = -\frac{t''}{2}(\alpha_3')^2, \tag{A45}$$

$$\tau_{dd}^{(18)} = -\frac{t'}{4}(\alpha_3')^2, \tau_{pd}^{(18)} = -\frac{t'}{2\sqrt{2}}(\alpha_3')^2,$$

$$\tau_{pp}^{(18)} = -\frac{t'}{2}(\alpha_3')^2, \tag{A46}$$

$$\iota_{dd}^{(19)} = -\frac{J}{8}\left[(\alpha_3')^2 + 2\sum_{\mu=4} 3^{\mu-4}(\alpha_\mu')^2\right],$$

$$\iota_{pp}^{(19)} = -\frac{J}{4}\left[(\alpha_3')^2 + 2\sum_{\mu=4} 3^{\mu-4}(\alpha_\mu')^2\right], \tag{A47}$$

$$\tau_{sd}^{(21)} = \frac{t}{2}\alpha_3'\alpha_2, \tau_{dd}^{(21)} = -\frac{t}{4}\alpha_3'\alpha_2',$$

$$\tau_{pd}^{(21)} = -\frac{t}{2\sqrt{2}}\alpha_3'\alpha_2', \tau_{sp}^{(21)} = \frac{t}{\sqrt{2}}\alpha_3'\alpha_2,$$

$$\tau_{pp}^{(21)} = -\frac{t}{2}\alpha_3'\alpha_2', \tag{A48}$$

$$\tau_{dd}^{(22)} = -\frac{t'}{4}(\alpha_3')^2, \tag{A49}$$

$$\tau_{pd}^{(23)} = -\frac{t'}{2\sqrt{2}}(\alpha_3')^2, \tau_{pp}^{(23)} = -\frac{t'}{2}(\alpha_3')^2, \tag{A50}$$

and

$$\omega_{dd}^{(1)} = -\frac{(\alpha_3')^2 + 2\sum_{\mu=4} 3^{\mu-4}(\alpha_\mu')^2}{4},$$

$$\omega_{pd}^{(1)} = -\frac{(\alpha_3')^2 + 2\sum_{\mu=4} 3^{\mu-4}(\alpha_\mu')^2}{2\sqrt{2}},$$

$$\omega_{pp}^{(1)} = -\frac{(\alpha_3')^2 + 2\sum_{\mu=4} 3^{\mu-4}(\alpha_\mu')^2}{2}. \tag{A51}$$

APPENDIX B: OPTICAL CONDUCTIVITY OF DOPED ANTIFERROMAGNETS

The optical spectrum evaluated by us is determined by following contributions to matrix elements: $\delta^{(n)}\langle\Psi_{\mathbf{R}_i}^{(o',0)}|j_x|\Psi_{\mathbf{R}=\mathbf{0}}^{(o),0}\rangle \equiv s_{o',o}^{(n)}(\mathbf{R}_i)$, where n labels different contributions,

$$s_{p_x,s}^{(1)}(\mathbf{0}) = -2it\sum_{\mu=0} \alpha_\mu\alpha_{\mu+1}'/\sqrt{2},$$

$$s_{s,p_x}^{(1)}(\mathbf{0}) = -2it\sum_{\mu=1} \alpha_\mu'\alpha_{\mu+1}/\sqrt{2},$$

$$s_{d,p_x}^{(1)}(\mathbf{0}) = -2it\sum_{\mu=1} \alpha_\mu'\alpha_{\mu+1}'/(2\sqrt{2}),$$

$$s_{p_x,d}^{(1)}(\mathbf{0}) = s_{d,p_x}^{(1)}(\mathbf{0}), \tag{B1}$$

$$s_{p_x,s}^{(2)}(\mathbf{0}) = 2it\sum_{\mu=2} \alpha_\mu\alpha_{\mu-1}'/\sqrt{2},$$

$$s_{s,p_x}^{(2)}(\mathbf{0}) = 2it\sum_{\mu=1} \alpha_\mu'\alpha_{\mu-1}/\sqrt{2},$$

$$s_{d,p_x}^{(2)}(\mathbf{0}) = -2it\sum_{\mu=2} \alpha_\mu'\alpha_{\mu-1}'/(2\sqrt{2}),$$

$$s_{p_x,d}^{(2)}(\mathbf{0}) = s_{d,p_x}^{(2)}(\mathbf{0}), \tag{B2}$$

$$s_{s,s}^{(3)}(\hat{\mathbf{x}} \pm \hat{\mathbf{y}}) = -it'\alpha_0^2, \tag{B3}$$

$$s_{s,s}^{(4)}(-\hat{\mathbf{x}} \pm \hat{\mathbf{y}}) = -s_{s,s}^{(3)}(\hat{\mathbf{x}} + \hat{\mathbf{y}}), \tag{B4}$$

$$s_{s,p_x}^{(5)}(\mathbf{0}) = 4it'\alpha_1'\alpha_1/\sqrt{2},$$

$$s_{d,p_x}^{(5)}(\mathbf{0}) = -4it'(\alpha_1')^2/(2\sqrt{2}), \tag{B5}$$

$$s_{p_x,s}^{(6)}(\mathbf{0}) = -s_{s,p_x}^{(5)}(\mathbf{0}),$$

$$s_{p_x,d}^{(6)}(\mathbf{0}) = s_{d,p_x}^{(5)}(\mathbf{0}), \tag{B6}$$

$$s_{s,s}^{(7)}(2\hat{\mathbf{x}}) = -2it''\alpha_0^2,$$

$$s_{s,s}^{(7)}(-2\hat{\mathbf{x}}) = -s_{s,s}^{(7)}(2\hat{\mathbf{x}}), \tag{B7}$$

$$s_{p_x,s}^{(8)}(\mathbf{0}) = -4it''\alpha_1\alpha_1'/\sqrt{2},$$

$$s_{s,p_x}^{(8)}(\mathbf{0}) = -s_{p_x,s}^{(8)}(\mathbf{0}),$$

$$s_{d,p_x}^{(8)}(\mathbf{0}) = 4it''(\alpha_1')^2/(2\sqrt{2}),$$

$$s_{p_x,d}^{(8)}(\mathbf{0}) = -s_{d,p_x}^{(8)}(\mathbf{0}). \tag{B8}$$

For example, contributions 1 and 2 are related to shortening and elongating strings by the current operator [Fig. 11], while contributions 3 and 4 to shifts between next NN sites [Figs. 13(a) and 13(b)]. We have considered processes involving strings of length up to two for matrix elements of the t term in the current operator and up to one for matrix elements of t' and t'' terms.

[1] J. Hubbard, Proc. R. Soc. London, Ser. A **277**, 237 (1964); **281**, 401 (1964).
[2] J. Kanamori, Prog. Theor. Phys. **30**, 275 (1963).
[3] B. O. Wells, Z.-X. Shen, A. Matsuura, D. M. King, M. A. Kastner, M. Greven, and R. J. Birgeneau, Phys. Rev. Lett. **74**, 964 (1995).
[4] S. A. Trugman, Phys. Rev. B **37**, 1597 (1988).
[5] B. Kyung and R. A. Ferrell, Phys. Rev. B **54**, 10125 (1996).
[6] F. Lema, and A. A. Aligia, Phys. Rev. B **55**, 14092 (1997).
[7] A. L. Chernyshev, A. V. Dotsenko, and O. P. Sushkov, Phys. Rev. B **49**, 6197 (1994).
[8] V. I. Belinicher, A. L. Chernyshev, A. V. Dotsenko, and O. P. Sushkov, Phys. Rev. B **51**, 6076 (1995).
[9] J. Bała, A. M. Oleś, and J. Zaanen, Phys. Rev. B **52**, 4597 (1995).
[10] N. M. Plakida, V. S. Oudovenko, P. Horsch, and A. I. Liechtenstein, Phys. Rev. B **55**, R11997 (1997).
[11] V. I. Belinicher, A. L. Chernyshev, and V. A. Shubin, Phys. Rev. B **56**, 3381 (1997).
[12] O. P. Sushkov, G. A. Sawatzky, R. Eder, and H. Eskes, Phys. Rev. B **56**, 11769 (1997).
[13] A. Damascelli, Z. Hussain, and Z.-X. Shen, Rev. Mod. Phys. **75**, 473 (2003).
[14] F. Ronning, C. Kim, D. L. Feng, D. S. Marshall, A. G. Loeser, L. L. Miller, J. N. Eckstein, L. Bozovic, and Z.-X. Shen, Science **282**, 2067 (1998).
[15] R. Eder and Y. Ohta, Phys. Rev. Lett. **72**, 2816 (1994).
[16] C. T. Chen, F. Sette, Y. Ma, M. S. Hybertsen, E. B. Stechel, W. M. C. Foulkes, M. Schluter, S.-W. Cheong, A. S. Cooper, L. W. Rupp, B. Batlogg, Y. L. Soo, Z. H. Ming, A. Krol, and Y. H. Kao, Phys. Rev. Lett. **66**, 104 (1991).
[17] R. Eder, Y. Ohta, and G. A. Sawatzky, Phys. Rev. B **55**, R3414 (1997).
[18] J. G. Storey, J. L. Tallon, G. V. M. Williams, and J. W. Loram, Phys. Rev. B **76**, 060502(R) (2007).
[19] Y. Kohsaka, T. Sasagawa, F. Ronning, T. Yoshida, C. Kim, T. Hanaguri, M. Azuma, M. Takano, Z.-X. Shen, and H. Takagi, J. Phys. Soc. Jpn. **72**, 1018 (2003).
[20] J. Chang, Y. Sassa, S. Guerrero, M. Mansson, M. Shi, S. Pailhes, A. Bendounan, R. Mottl, T. Claesson, O. Tjernberg, L. Patthey, M. Ido, N. Momono, M. Oda, C. Mudry, and J. Mesot, arXiv:0805.0302 (unpublished).
[21] S. A. Trugman, Phys. Rev. Lett. **65**, 500 (1990).
[22] N. P. Ong, Z. Z. Wang, J. Clayhold, J. M. Tarascon, L. H. Greene, and W. R. McKinnon, Phys. Rev. B **35**, 8807 (1987).
[23] H. Takagi, T. Ido, S. Ishibashi, M. Uota, S. Uchida, and Y. Tokura, Phys. Rev. B **40**, 2254 (1989).
[24] R. Eder, Y. Ohta, and T. Shimozato, Phys. Rev. B **50**, 3350 (1994).
[25] N. Doiron-Leyraud, C. Proust, D. LeBoeuf, J. Levallois, J.-B. Bonnemaison, R. Liang, D. A. Bonn, W. N. Hardy, and L. Taillefer, Nature (London) **447**, 565 (2007).
[26] E. A. Yelland, J. Singleton, C. H. Mielke, N. Harrison, F. F. Balakirev, B. Dabrowski, and J. R. Cooper, Phys. Rev. Lett. **100**, 047003 (2008).
[27] A. F. Bangura, J. D. Fletcher, A. Carrington, J. Levallois, M. Nardone, B. Vignolle, P. J. Heard, N. Doiron-Leyraud, D. LeBoeuf, L. Taillefer, S. Adachi, C. Proust, and N. E. Hussey, Phys. Rev. Lett. **100**, 047004 (2008).
[28] D. LeBoeuf, N. Doiron-Leyraud, J. Levallois, R. Daou, J.-B. Bonnemaison, N. E. Hussey, L. Balicas, B. J. Ramshaw, R. Liang, D. A. Bonn, W. N. Hardy, S. Adachi, C. Proust, and L. Taillefer, Nature (London) **450**, 533 (2007).
[29] R. Eder and Y. Ohta, Phys. Rev. B **51**, 6041 (1995).
[30] P. W. Leung, Phys. Rev. B **73**, 014502 (2006).
[31] E. Dagotto and J. R. Schrieffer, Phys. Rev. B **43**, 8705 (1991).
[32] R. Eder and Y. Ohta, Phys. Rev. B **50**, 10043 (1994).
[33] R. Eder, Y. Ohta, and S. Maekawa, Phys. Rev. Lett. **74**, 5124 (1995).
[34] M. Vojta and K. W. Becker, Europhys. Lett. **38**, 607 (1997).
[35] R. Eder and Y. Ohta, Phys. Rev. B **51**, 11683 (1995).
[36] K. A. Chao, J. Spałek, and A. M. Oleś, Phys. Rev. B **18**, 3453 (1978).
[37] F. C. Zhang and T. M. Rice, Phys. Rev. B **37**, 3759 (1988).
[38] A. Nazarenko, K. J. E. Vos, S. Haas, E. Dagotto, and R. J. Gooding, Phys. Rev. B **51**, 8676 (1995).
[39] P. W. Leung, B. O. Wells, and R. J. Gooding, Phys. Rev. B **56**, 6320 (1997).
[40] R. Eder and K. W. Becker, Z. Phys. B: Condens. Matter **78**, 219 (1990).
[41] R. Eder and K. W. Becker, Phys. Rev. B **44**, 6982 (1991).
[42] R. Eder and P. Wróbel, Phys. Rev. B **47**, 6010 (1993).
[43] R. Eder, P. Wróbel, and Y. Ohta, Phys. Rev. B **54**, R11034 (1996).
[44] P. Wróbel and R. Eder, Phys. Rev. B **58**, 15160 (1998).
[45] J. Inoue and S. Maekawa, J. Phys. Soc. Jpn. **59**, 2110 (1990).
[46] M. Vojta and K. W. Becker, Phys. Rev. B **57**, 3099 (1998).
[47] J. Bonča, S. Maekawa, and T. Tohyama, Phys. Rev. B **76**, 035121 (2007).
[48] M. Vojta and K. W. Becker, Phys. Rev. B **54**, 15483 (1996).
[49] G. Martinez and P. Horsch, Phys. Rev. B **44**, 317 (1991).
[50] Z. Liu and E. Manousakis, Phys. Rev. B **45**, 2425 (1992).
[51] E. Manousakis, Phys. Rev. B **75**, 035106 (2007).
[52] W. E. Spicer, Phys. Rev. **112**, 114 (1958).
[53] C. Caroli, D. Lederer-Rozenblatt, B. Roulet, and D. Saint-James, Phys. Rev. B **8**, 4552 (1973).
[54] G. F. Reiter, Phys. Rev. B **49**, 1536 (1994).
[55] J. Eroles, C. D. Batista, and A. A. Aligia, Phys. Rev. B **59**, 14092 (1999).
[56] K. M. Shen, F. Ronning, W. Meevasana, D. H. Lu, N. J. C. Ingle, F. Baumberger, W. S. Lee, L. L. Miller, Y. Kohsaka, M. Azuma, M. Takano, H. Takagi, and Z. X. Shen, Phys. Rev. B **75**, 075115 (2007).
[57] F. Ronning, K. M. Shen, N. P. Armitage, A. Damascelli, D. H. Lu, Z.-X. Shen, L. L. Miller, and C. Kim, Phys. Rev. B **71**, 094518 (2005).
[58] J. J. M. Pothuizen, R. Eder, N. T. Hien, M. Matoba, A. A. Menovsky, and G. A. Sawatzky, Phys. Rev. Lett. **78**, 717 (1997).
[59] J. Graf, G.-H. Gweon, K. McElroy, S. Y. Zhou, C. Jozwiak, E. Rotenberg, A. Bill, T. Sasagawa, H. Eisaki, S. Uchida, H. Takagi, D.-H. Lee, and A. Lanzara, Phys. Rev. Lett. **98**, 067004 (2007).
[60] B. P. Xie *et al.*, Phys. Rev. Lett. **98**, 147001 (2007).
[61] T. Valla, T. E. Kidd, W.-G. Yin, G. D. Gu, P. D. Johnson, Z.-H. Pan, and A. V. Fedorov, Phys. Rev. Lett. **98**, 167003 (2007).
[62] Z.-H. Pan, P. Richard, A. V. Fedorov, T. Kondo, T. Takeuchi, S. L. Li, Pengcheng Dai, G. D. Gu, W. Ku, Z. Wang, and H. Ding, arXiv:cond-mat/0610442 (unpublished).
[63] J. Chang, S. Pailhes, M. Shi, M. Manson, T. Claesson, O. Tjernberg, J. Voigt, V. Perez, L. Patthey, N. Momono, M. Oda, M.

Ido, A. Schnyder, C. Mudry, and J. Mesot, Phys. Rev. B **75**, 224508 (2007).
[64] D. S. Inosov, J. Fink, A. A. Kordyuk, S. V. Borisenko, V. B. Zabolotnyy, R. Schuster, M. Knupfer, B. Buchner, R. Follath, H. A. Durr, W. Eberhardt, V. Hinkov, B. Keimer, and H. Berger, Phys. Rev. Lett. **99**, 237002 (2007).
[65] D. E. Eastman and J. L. Freeouf, Phys. Rev. Lett. **34**, 395 (1975).
[66] E. Dagotto, F. Ortolani, and D. Scalapino, Phys. Rev. B **46**, 3183 (1992).
[67] H. Eskes and R. Eder, Phys. Rev. B **54**, R14226 (1996).
[68] C. Gröber, R. Eder, and W. Hanke, Phys. Rev. B **62**, 4336 (2000).
[69] S.-J. Oh, J. W. Allen, I. Lindau, and J. C. Mikkelsen, Jr., Phys. Rev. B **26**, 4845 (1982).
[70] M. M. Zemljič, P. Prelovšek, and T. Tohyama, Phys. Rev. Lett. **100**, 036402 (2008).
[71] S. Uchida, T. Ido, H. Takagi, T. Arima, Y. Tokura, and S. Tajima, Phys. Rev. B **43**, 7942 (1991).
[72] J. Hwang, E. J. Nicol, T. Timusk, A. Knigavko, and J. P. Carbotte, Phys. Rev. Lett. **98**, 207002 (2007).